



Systematic Fitting and Comparison of Hyperelastic Continuum Models for Elastomers

Alexander Ricker^{1,2} · Peter Wriggers¹

Received: 2 May 2022 / Accepted: 6 December 2022 / Published online: 9 January 2023
© The Author(s) 2023

Abstract

Hyperelasticity is a common modeling approach to reproduce the nonlinear mechanical behavior of rubber materials at finite deformations. It is not only employed for stand-alone, purely elastic models but also within more sophisticated frameworks like viscoelasticity or Mullins-type softening. The choice of an appropriate strain energy function and identification of its parameters is of particular importance for reliable simulations of rubber products. The present manuscript provides an overview of suitable hyperelastic models to reproduce the isochoric as well as volumetric behavior of nine widely used rubber compounds. This necessitates firstly a discussion on the careful preparation of the experimental data. More specific, procedures are proposed to properly treat the preload in tensile and compression tests as well as to proof the consistency of experimental data from multiple experiments. Moreover, feasible formulations of the cost function for the parameter identification in terms of the stress measure, error type as well as order of the residual norm are studied and their effect on the fitting results is illustrated. After these preliminaries, invariant-based strain energy functions with decoupled dependencies on all three principal invariants are employed to identify promising models for each compound. Especially, appropriate parameter constraints are discussed and the role of the second invariant is analyzed. Thus, this contribution may serve as a guideline for the process of experimental characterization, data processing, model selection and parameter identification for existing as well as new materials.

1 Introduction

Elasticity describes an idealized mechanical material behavior whose stress response depends only on the current deformation state. Once the external load is removed, the material is expected to recover its initial, undeformed configuration and to release the entire work done by the external load, i.e., no hysteretic effects occur. The concept of hyperelasticity ensures such a behavior by defining the material response in terms of a potential (commonly called strain energy density function W) from which the constitutive equations are derived. Thus, a path independent mechanical work is

guaranteed and the relation between the stress and deformation tensor is provided by a scalar function that is conveniently to handle. Furthermore, the laws of thermodynamics can readily be evaluated and a variational functional for the balance of the linear momentum can be formulated. As a consequence of these desirable properties, hyperelasticity is a common modeling approach in solid mechanics. Especially materials that can undergo large deformations, like elastomers or soft tissues, are typically described by a strain energy function.

In the literature, a vast number of strain energy functions have been published, particularly for rubber materials at finite strains. However, their validity is rarely tested for different rubber types or compounds such that an extensive database for a well-founded model selection is missing. Moreover, most publications focus on modeling either the isochoric response or, less often, the volumetric behavior. Also review articles which compile lists and benchmark tests of strain energy functions for rubbers are limited to a few compounds and often stick to the classical Treloar [95] or Kawabata data [56] stemming from sulfur crosslinked natural and isoprene rubber, respectively. An overview of these

✉ Alexander Ricker
ricker@ikm.uni-hannover.de

Peter Wriggers
ricker@ikm.uni-hannover.de

¹ Institute of Continuum Mechanics, Leibniz Universität Hannover, An der Universität 1, 30823 Garbsen, Germany

² Department Simulation and Continuum Mechanics, Deutsches Institut für Kautschuktechnologie e.V., Eupener Straße 33, 30519 Hannover, Germany

Table 1 Review articles on isochoric hyperelastic models for rubber materials (number of models n includes only models for rubbers; CB: carbon black, HNBR: hydrogenated nitrile butadiene rubber, NR: natural rubber, S: sulfur, Si: silicone)

Literature	n	Experimental data	Objective
[37]	10	None	Deriving a new model
[34]	8	4 S-crosslinked NR from literature	Visual comparison, giving attention to small strain behavior, considering applicability of Valanis-Landel hypothesis
[103]	5	S-crosslinked NR	Discussing the models' capability and drawbacks, considering also swollen rubber, proposing a model extension to improve the fitting at small strain
[13]	8	Treloar data	Visual comparison, discussing predictivity to other deformation modes, addressing the effects of compressibility
[88]	6	lowly CB-filled HNBR	Visual comparison, considering conditioned and unconditioned state, discussing predictivity to other deformation modes, studying of finite element simulations
[96]	45	none	Providing list of references
[46]	5	none	Discussing behavior at large strains, presenting extensions to thermoelasticity, anisotropy and compressibility
[70]	7	Si-rubber	Visual comparison and in terms of the correlation coefficient, considering also pig muscular tissue
[68]	20	Treloar & Kawabata data	Compiling rankings
[47]	25	Treloar data & NR & Si-rubber from [71]	Grading of the model performance, deriving a new model
[91] & [48]	14 & 11	Treloar data	Providing and testing consistent linearizations, discussing performance and predictivity to other deformation modes
[11]	25	Treloar data & S-crosslinked NR from [104]	Presenting building-strategy for new models
[49]	8	Treloar data	Considering micromechanically motivated chain and network models, visual comparison, studying predictivity to other deformation modes
[33]	8	Treloar data	Developing an application for parameter identification and verification
[74]	12	Treloar data	Modeling of nonlinear elasticity using deformation dependent parameters
[22]	44	Treloar & Kawabata data	Compiling rankings, discussing alternative cost functions with weights for each experiment, presenting a generic fitting algorithm, discussing predictivity to other deformation modes
[30]	7	2 CB-filled, S-crosslinked NRs	Proposing a new model, analyzing temperature dependencies
[41]	75	Treloar data & CB-filled HNBR from [45]	Compiling top ten rankings, comparing run time of finite element simulations

Table 2 Review articles on volumetric hyperelastic models (n is the number of models; CB: carbon black, EPDM: ethylene propylene diene rubber, S: sulfur)

Literature	n	Experimental data	Objective
[66]	5	None	Discussing constraints on volumetric strain energy functions
[26]	5	None	Discussing constraints on volumetric strain energy functions, proposing new models
[38]	10	None	Discussing polyconvexity (also for isochoric models), proposing new models
[83]	4	CB-filled, S-crosslinked EPDM	Illustrating the effect of CB content, crosslink content and curing time on the bulk modulus

articles is given in Tables 1 and 2 including the number of considered models, the type of rubber used for fitting as well as the objective of the work.

The present manuscript provides a systematic fitting of both, isochoric and volumetric hyperelastic models. They are fitted to the experimental data of nine different rubber compounds and, thus, an extensive database is established. In

addition and in contrast to the existing literature, the dependence of the strain energy functions on the first and second principal invariant is investigated. Particularly, the role and importance of the second principal invariant for rubber models is studied in detail. Also, the effects of possible cost function formulations on the fitting results are demonstrated,

reasonable constraints on the parameter bounds are recapped and crucial model properties are highlighted.

Another difference between the present work and existing contributions is that the treatment of the experimental data is highlighted. Since an accurate parameter identification requires a careful preparation of the raw test data, some common issues regarding data processing are addressed. On the one hand, a physically based approach is outlined to consider the preload in biaxial tensile tests as well as compression tests. On the other hand, a straightforward method is proposed to check the consistency between data stemming from multiple experiments.

The manuscript is organized as follows. First, the theoretical foundations are laid in Sect. 2 including continuum mechanics, thermodynamics, the experimental setup and parameter identification. Next in Sect. 3, the treatment of the experimental data is explained. Finally in Sects. 4 and 5, the fitting procedure for the isochoric and volumetric strain energy functions is outlined, conducted and discussed.

2 Theory of Hyperelasticity and Experimental Methods

2.1 Kinematics

To describe the deformation of a solid body, the motion of a material point is tracked. Denoting its position in a reference configuration (typically the undeformed state) and the current configuration by \mathbf{X} and $\mathbf{x}(\mathbf{X}, t)$, respectively, the displacement $\mathbf{u} = \mathbf{x} - \mathbf{X}$ is introduced. Then, the deformation gradient

$$\mathbf{F} = \frac{\partial \mathbf{u}}{\partial \mathbf{X}} + \mathbf{I} \tag{1}$$

is computed which is an invertible, two-field tensor. \mathbf{I} denotes the identity tensor.

Rotational and distortional contributions to the deformation gradient are separated by the polar decomposition

$$\mathbf{F} = \mathbf{R} \cdot \mathbf{U} \tag{2}$$

with the proper orthogonal rotation \mathbf{R} and the symmetric right stretch tensor \mathbf{U} . Moreover, \mathbf{U} can be split into a volume-preserving deformation and a pure dilatation represented by the isochoric (i.e., unimodular) right stretch tensor $\bar{\mathbf{U}} = J^{-1/3} \mathbf{U}$ and the volumetric contribution $J^{1/3} \mathbf{I}$, respectively. Here, $J = \det(\mathbf{U})$ denotes the determinant of \mathbf{U} and measures the local volume change. Note that $\det(\mathbf{F}) = \det(\mathbf{U})$ holds true due to the multiplicativity of the determinant and $\det(\mathbf{R}) = 1$. The multiplicative decomposition of the deformation gradient yields

$$\mathbf{F} = \mathbf{R} \cdot \bar{\mathbf{U}} J^{1/3}. \tag{3}$$

The square of \mathbf{U} is called right Cauchy-Green tensor

$$\mathbf{C} = \mathbf{U}^2 = \mathbf{F}^T \cdot \mathbf{F} \tag{4}$$

whose principal invariants are

$$\begin{aligned} I_1 &= \text{tr}(\mathbf{C}) = \|\mathbf{F}\|^2, & I_2 &= \text{tr}(\text{adj}(\mathbf{C})) = \|\text{adj}(\mathbf{F})\|^2, \\ I_3 &= \det(\mathbf{C}) = \det(\mathbf{F})^2 \end{aligned} \tag{5}$$

with the trace $\text{tr}(\cdot)$, adjugate $\text{adj}(\cdot) = \det(\cdot)(\cdot)^{-1}$ and Frobenius norm $\|\cdot\|$. Accordingly, the square of $\bar{\mathbf{U}}$ will be referred to as isochoric right Cauchy-Green tensor

$$\bar{\mathbf{C}} = \bar{\mathbf{U}}^2 = \det(\mathbf{C})^{-1/3} \mathbf{C} \tag{6}$$

and the isochoric principal invariants are defined as

$$\begin{aligned} \bar{I}_1 &= \text{tr}(\bar{\mathbf{C}}) = I_1 I_3^{-1/3} \geq 3, \\ \bar{I}_2 &= \text{tr}(\text{adj}(\bar{\mathbf{C}})) = \text{tr}(\bar{\mathbf{C}}^{-1}) = I_2 I_3^{-2/3} \geq 3. \end{aligned} \tag{7}$$

The eigenvalues of \mathbf{U} are called principal stretches and denoted by $\lambda_1, \lambda_2, \lambda_3$ whereas the eigenvalues of $\bar{\mathbf{U}}$ will be referred to as isochoric stretches $\bar{\lambda}_k = J^{-1/3} \lambda_k, k = 1, 2, 3$. Both stretch tensors (and their squares) share the same eigenvectors \mathbf{G}_k , viz.,

$$\mathbf{U} = \sum_{k=1}^3 \lambda_k \mathbf{G}_k \otimes \mathbf{G}_k, \quad \bar{\mathbf{U}} = \sum_{k=1}^3 \bar{\lambda}_k \mathbf{G}_k \otimes \mathbf{G}_k. \tag{8}$$

2.2 Stresses

The Cauchy stress $\boldsymbol{\sigma}$ (also known as true stress) is defined as force per unit current area. More precisely, the stress tensor relates the normal \mathbf{n} of an imaginary cut surface da in the current configuration and the resultant force $d\mathbf{f}$ acting on the cutting surface such that

$$\boldsymbol{\sigma} \cdot \mathbf{n} = \frac{d\mathbf{f}}{da}. \tag{9}$$

In contrast, the 1st Piola-Kirchhoff stress \mathbf{P} (also known as engineering stress) describes the force per unit reference area, viz.,

$$\mathbf{P} \cdot \mathbf{N} = \frac{d\mathbf{f}}{dA} \tag{10}$$

where \mathbf{N} and dA are the corresponding normal vector and cutting surface in the reference configuration. The 1st Piola-Kirchhoff stress is a two-field tensor, work-conjugated to the material time derivative of the deformation gradient $\dot{\mathbf{F}}$ and linked to the Cauchy stress by

$$P = J \sigma \cdot F^{-T} \tag{11}$$

with the transposed inverse $(\cdot)^{-T}$. The third stress measure used in this manuscript is the 2nd Piola-Kirchhoff stress S which is work-conjugated to $1/2 \dot{C}$. It is based in the reference configuration, lacks a physical meaning and can be computed by

$$S = J F^{-1} \cdot \sigma \cdot F^{-T} = F^{-1} \cdot P. \tag{12}$$

The Cauchy stress can be additively decomposed into an isochoric (i.e., traceless) and a volumetric contribution σ_{iso} and σ_{vol} , respectively, commonly called deviatoric and hydrostatic stress. They are given by

$$\begin{aligned} \sigma_{\text{iso}} &= \sigma - \sigma_{\text{vol}} \quad \text{and} \quad \sigma_{\text{vol}} = -pI \quad \text{with} \\ p &= -\frac{\text{tr}(\sigma)}{3} \end{aligned} \tag{13}$$

where p is called hydrostatic pressure. Applying Eq. (12) to the deviatoric and hydrostatic Cauchy stress leads to

$$S_{\text{iso}} = S - S_{\text{vol}} \quad \text{and} \quad S_{\text{vol}} = -pJC^{-1} \quad \text{with} \quad p = -\frac{\text{tr}(C \cdot S)}{3J}. \tag{14}$$

The stress power per unit reference volume is given by

$$P = S : \frac{1}{2} \dot{C} = \frac{1}{2} S_{ij} \dot{C}_{ij}. \tag{15}$$

In analogous manner to the stress, it splits additively into an isochoric and a volumetric part, viz.,

$$P_{\text{iso}} = P - P_{\text{vol}} \quad \text{and} \quad P_{\text{vol}} = -p\dot{J} \tag{16}$$

where the identity $\dot{J} = J/2 C^{-1} : \dot{C}$ is used.

2.3 Thermodynamics

The second law of thermodynamics for isothermal conditions can be represented via the Clausius-Planck inequality per unit reference volume

$$D_m = P - \dot{\Psi} \geq 0 \tag{17}$$

with the mechanical dissipation rate D_m and the free energy per unit reference volume Ψ . For hyperelasticity, the free energy is given by a strain energy density function W . Assuming that W is defined in terms of the right Cauchy-Green tensor, the chain rule $\dot{W} = \partial W / \partial C : \dot{C}$ and Eq. (15) can be applied resulting in

$$D_m = \left(S - 2 \frac{\partial W}{\partial C} \right) : \frac{1}{2} \dot{C} \geq 0. \tag{18}$$

Thus, the Clausius-Planck inequality is always fulfilled by defining the stress-deformation relation

$$\begin{aligned} S &= 2 \frac{\partial W}{\partial C} \quad \Rightarrow \quad P = 2F \cdot \frac{\partial W}{\partial C}, \\ \sigma &= \frac{2}{J} F \cdot \frac{\partial W}{\partial C} \cdot F^T, \end{aligned} \tag{19}$$

cf. Eq. (12), implying a material behavior free of dissipation, i.e., $D_m = 0$.

2.4 Strain Energy Density Functions and Imposed Restrictions

The strain energy functions discussed in this manuscript are assumed to be composed of an isochoric part W_{iso} in terms of the isochoric invariants \bar{I}_1, \bar{I}_2 and a volumetric part W_{vol} depending on the volume change J , viz.,

$$W = W_{\text{iso}}(\bar{I}_1, \bar{I}_2) + W_{\text{vol}}(J). \tag{20}$$

Such a separate modeling of the deviatoric and the hydrostatic response is a reasonable and widely used approach for nearly incompressible materials like elastomers¹. Employing Eq. (19)₁ with the isochoric-volumetric split of the strain energy according to Eq. (20) leads automatically to a decoupled stress response, cf. Eq. (14). With the derivatives $\partial \bar{I}_1 / \partial C = \text{dev}(\bar{C}) \cdot C^{-1}$, $\partial \bar{I}_2 / \partial C = -\text{dev}(\bar{C}^{-1}) \cdot C^{-1}$ and $\partial J / \partial C = J/2 C^{-1}$ the stress contributions read

$$\begin{aligned} S_{\text{iso}} &= 2 \text{dev} \left(\frac{\partial W_{\text{iso}}}{\partial \bar{I}_1} \bar{C} - \frac{\partial W_{\text{iso}}}{\partial \bar{I}_2} \bar{C}^{-1} \right) \cdot C^{-1} \quad \text{and} \\ S_{\text{vol}} &= -pJC^{-1} \quad \text{with} \quad p = -\frac{\partial W_{\text{vol}}}{\partial J} \end{aligned} \tag{21}$$

where $\text{dev}(\cdot)$ denotes the traceless part of a tensor, cf. App. A for a representation in the current configuration. Furthermore, the authors restrict themselves to strain energy functions of a fully decoupled form

$$W = W_{\text{iso},1}(\bar{I}_1) + W_{\text{iso},2}(\bar{I}_2) + W_{\text{vol}}(J), \tag{22}$$

what is motivated by a separate investigation of the \bar{I}_1 - and \bar{I}_2 -terms, see Sects. 4.1.1 and 4.1.2 for a detailed explanation.

An alternative form of a decoupled strain energy is obtained by defining the isochoric part of Eq. (20) in terms of the isochoric stretches $\bar{\lambda}_k$. To satisfy a priori symmetry requirements due to isotropy, the Valanis-Landel assumption [97] is employed leading to the form

$$W_{\text{iso}}(\bar{\lambda}_1, \bar{\lambda}_2, \bar{\lambda}_3) = \sum_{k=1}^3 \omega(\bar{\lambda}_k) \tag{23}$$

¹ Note that the pressure dependent stress response of filled rubbers, as shown for instance by [17], can not be captured by a decoupled modeling approach.

such that all three stretches are treated uniformly and separately by a scalar function ω , cf. [53, 98, 55] for the validity and limitations of this assumption regarding experimental findings. The corresponding 2nd Piola-Kirchhoff stress is obtained as

$$S_{\text{iso}} = \text{dev} \left(\sum_{k=1}^3 \frac{\partial \omega}{\partial \bar{\lambda}_k} \bar{\lambda}_k \mathbf{G}_k \otimes \mathbf{G}_k \right) \cdot \mathbf{C}^{-1} \quad (24)$$

see for instance [80]. The forms $W_{\text{iso}}(\bar{I}_1, \bar{I}_2)$ and $W_{\text{iso}}(\bar{\lambda}_1, \bar{\lambda}_2, \bar{\lambda}_3)$ will be referred to as invariant and stretch formulation, respectively.

The second law of thermodynamics, cf. Sect. 2.3, does not impose any restrictions on the construction of the strain energy function. Therefore, many authors discussed requirements for an objective, physically plausible and numerically desirable material behavior. Objectivity is a very fundamental demand for material frame indifference, see for instance [39]. It is automatically satisfied by an appropriate choice of arguments of the strain energy function, e.g., the invariants in Eq. (20) or the eigenvalues in Eq. (23). Physically motivated restrictions stem from experimental or empirical observations, e.g.,

- Greater stress occurs always in the direction of the greater strain, Baker-Ericksen inequalities [5]
- Incremental mechanical work done by external loads must be positive, Drucker-Hill postulate [28, 44]
- Tangential shear and bulk modulus must be positive
- Sound speed in a material must be a non-complex number

These wordings must then be turned into verifiable mathematical formulations within the finite strain theory and typically lead to constraints on the set of feasible parameters. Also constraints when approaching certain limits or deformation states, e.g., $J \rightarrow 0 \Rightarrow W \rightarrow \infty$ or $W(\mathbf{F} = \mathbf{I}) = W(\mathbf{F} = \mathbf{R}) < W(\mathbf{I} \neq \mathbf{F} \neq \mathbf{R})$ are mostly based on physical considerations. On the other hand, numerical restrictions demand the existence or even uniqueness of a solution in elastostatics. They result for example in

- (Poly)convexity or ellipticity conditions for the strain energy function
- Monotonicity, invertibility or growth conditions for the stress-strain relation
- Positive definiteness conditions for the material tangent

See for instance [6, 7, 69, 77] for an overview and implications between these conditions. Since some of the numerical restrictions have a direct physical consequence, the boundary between both categories is blurred. Furthermore, a few restrictions do not even affect the constitutive equations but

are reasonable for convenience, e.g., normalization conditions like $W(\mathbf{F} = \mathbf{I}) = 0$.

The choice of a suitable restriction depends on the application and is often a trade-off between numerical stability and the implied limitations. For instance, [55, 9] showed experimentally that $\partial W / \partial \bar{I}_2 < 0$ for small biaxial deformations of natural rubber. Too strong restrictions can easily rule out the capability of a model to reproduce this behavior. Moreover, the demand for polyconvexity would preclude a priori several $W_{\text{iso},2}$ -functions from the study in this manuscript as [38] showed that \bar{I}_2^m is not a polyconvex term for $m < 3/2$. In addition, strict convexity of $W(\mathbf{F})$ is violated in the case of buckling or phase transitions. Sects. 4.1.1 and 5 discuss the restrictions made for each function $W_{\text{iso},1}(\bar{I}_1)$, $W_{\text{iso},2}(\bar{I}_2)$ and $W_{\text{vol}}(J)$.

2.5 Incompressibility

Nearly incompressible materials like rubbers and fluids are characterized by a stress response being much larger for volumetric deformations than for isochoric deformations. Thus, the material volume tends to remain nearly constant, viz., $J \approx 1$ and their Poisson ratio ν is close to 0.5. For analytical considerations, nearly incompressible materials are often assumed to be perfectly incompressible, i.e., $J = 1$ always holds true and $\nu = 0.5$. In this case, the stretch tensor \mathbf{U} and the isochoric stretch tensor $\bar{\mathbf{U}}$ as well as their invariants and eigenvalues coincide. Furthermore, the hydrostatic pressure p in Eq. (14) is not given by a constitutive equation as in Eq. (21) but is determined by the static equilibrium.

2.6 Deformation Modes for Material Characterization

The deformation and stress states of five frequently used experiments for the characterization of the mechanical material behavior of rubbers are considered in this work: uniaxial tension, pure shear (also known as planar tension), equibiaxial tension, simple shear and confined compression (also known as volumetric compression). These idealized deformation modes are illustrated in App. B.

The uniaxial tension, pure shear and equibiaxial tension state (denoted by ux, ps and bx) can be derived as special cases of the general biaxial deformation mode

$$\mathbf{F} = \mathbf{U} = \bar{\mathbf{U}} = \begin{bmatrix} \lambda_1 & 0 & 0 \\ 0 & \lambda_2 & 0 \\ 0 & 0 & \lambda_3 = \frac{1}{\lambda_1 \lambda_2} \end{bmatrix} \quad \text{and} \quad \mathbf{R} = \mathbf{I} \quad (25)$$

where $\lambda_1 = \lambda$ denotes the stretch in load direction x . The z -direction is considered as stress-free and the corresponding stretch $\lambda_3 = 1/(\lambda_1 \lambda_2)$ follows from the assumption of incompressibility. See Table 3 for the lateral stretch λ_2 in

Table 3 Hyperelastic stress response in deformation modes which are commonly used for experimental material characterization of rubber materials ($E_0^{\text{ux}}, E_0^{\text{ps}}, E_0^{\text{bx}}, G_0, M_0$ and K_0 are the initial Young, pure shear, equibiaxial, shear, longitudinal and bulk modulus; see App. C for the $\bar{I}_2(\bar{I}_1)$ -dependencies)

Deformation mode	Deformation gradient \mathbf{F}	Stress conversion	Invariant-based hyperelasticity	Stretch-based hyperelasticity
Incompressible uniaxial tension (ux)	$\begin{bmatrix} \lambda & 0 & 0 \\ 0 & 1/\sqrt{\lambda} & 0 \\ 0 & 0 & 1/\sqrt{\lambda} \end{bmatrix}$	$\begin{aligned} P_{xx} &= \frac{F_x}{A_x} \\ \sigma_{xx} &= \lambda P_{xx} \\ S_{xx} &= \frac{P_{xx}}{\lambda} \end{aligned}$	$\begin{aligned} \bar{I}_1 &= \lambda^2 + \frac{2}{\lambda} \quad \bar{I}_2 = 2\lambda + \frac{1}{\lambda^2} \quad J = 1 \\ P_{xx} &= 2 \left(\frac{\partial W}{\partial \bar{I}_1} + \frac{\partial W}{\partial \bar{I}_2} \frac{1}{\lambda} \right) \left(\lambda - \frac{1}{\lambda^2} \right) \\ E_0^{\text{ux}} &= 6 \left(\frac{\partial W}{\partial \bar{I}_1} + \frac{\partial W}{\partial \bar{I}_2} \right)_{\bar{I}_1=\bar{I}_2=3} \end{aligned}$	$\begin{aligned} \bar{\lambda}_1 &= \lambda \quad \bar{\lambda}_2 = \bar{\lambda}_3 = \frac{1}{\sqrt{\lambda}} \quad J = 1 \\ P_{xx} &= \omega'(\bar{\lambda}_1) - \omega'(\bar{\lambda}_3) \frac{1}{\sqrt{\lambda^3}} \\ E_0^{\text{ux}} &= \frac{3}{2} (\omega'(1) + \omega''(1)) \end{aligned}$
Pure shear (ps)/ incompressible planar tension	$\begin{bmatrix} \lambda & 0 & 0 \\ 0 & 1 & 0 \\ 0 & 0 & 1/\lambda \end{bmatrix}$	$\begin{aligned} P_{xx} &= \frac{F_x}{A_x} \\ \sigma_{xx} &= \lambda P_{xx} \\ S_{xx} &= \frac{P_{xx}}{\lambda} \end{aligned}$	$\begin{aligned} \bar{I}_1 = \bar{I}_2 &= \lambda^2 + \frac{1}{\lambda^2} + 1 \quad J = 1 \\ P_{xx} &= 2 \left(\frac{\partial W}{\partial \bar{I}_1} + \frac{\partial W}{\partial \bar{I}_2} \right) \left(\lambda - \frac{1}{\lambda^3} \right) \\ E_0^{\text{ps}} &= \frac{4}{3} E_0^{\text{ux}} \end{aligned}$	$\begin{aligned} \bar{\lambda}_1 &= \lambda \quad \bar{\lambda}_2 = 1 \quad \bar{\lambda}_3 = \frac{1}{\lambda} \quad J = 1 \\ P_{xx} &= \omega'(\bar{\lambda}_1) - \omega'(\bar{\lambda}_3) \frac{1}{\lambda^2} \\ E_0^{\text{ps}} &= \frac{4}{3} E_0^{\text{ux}} \end{aligned}$
Incompressible equibiaxial tension (bx)	$\begin{bmatrix} \lambda & 0 & 0 \\ 0 & \lambda & 0 \\ 0 & 0 & 1/\lambda^2 \end{bmatrix}$	$\begin{aligned} P_{xx} &= \frac{F_x}{A_x} \\ \sigma_{xx} &= \lambda P_{xx} \\ S_{xx} &= \frac{P_{xx}}{\lambda} \end{aligned}$	$\begin{aligned} \bar{I}_1 &= 2\lambda^2 + \frac{1}{\lambda^4} \quad \bar{I}_2 = \lambda^4 + \frac{2}{\lambda^2} \quad J = 1 \\ P_{xx} &= 2 \left(\frac{\partial W}{\partial \bar{I}_1} + \frac{\partial W}{\partial \bar{I}_2} \lambda^2 \right) \left(\lambda - \frac{1}{\lambda^5} \right) \\ E_0^{\text{bx}} &= 2 E_0^{\text{ux}} \end{aligned}$	$\begin{aligned} \bar{\lambda}_1 = \bar{\lambda}_2 &= \lambda \quad \bar{\lambda}_3 = \frac{1}{\lambda^2} \quad J = 1 \\ P_{xx} &= \omega'(\bar{\lambda}_1) - \omega'(\bar{\lambda}_3) \frac{1}{\lambda^3} \\ E_0^{\text{bx}} &= 2 E_0^{\text{ux}} \end{aligned}$
Simple shear (ss)	$\begin{bmatrix} 1 & s & 0 \\ 0 & 1 & 0 \\ 0 & 0 & 1 \end{bmatrix}$	$\begin{aligned} P_{xy} &= \frac{F_y}{A_y} \\ \sigma_{xy} &= P_{xy} \\ S_{xy} &= P_{xy} - s P_{yy} \\ P_{yy} &= \frac{F_y}{A_y} \end{aligned} \quad G_0 = \frac{1}{3} E_0^{\text{ux}}$	$\begin{aligned} \bar{I}_1 = \bar{I}_2 &= s^2 + 3 \quad J = 1 \\ P_{xy} &= 2 \left(\frac{\partial W}{\partial \bar{I}_1} + \frac{\partial W}{\partial \bar{I}_2} \right) s \end{aligned}$	$\begin{aligned} \bar{\lambda}_1 &= \frac{1}{2} \left(\sqrt{s^2 + 4} + s \right) \quad \bar{\lambda}_2 = 1 \\ \bar{\lambda}_3 &= \frac{1}{2} \left(\sqrt{s^2 + 4} - s \right) \quad J = 1 \\ P_{xy} &= \frac{\omega'(\bar{\lambda}_1)(2+s\bar{\lambda}_1) - \omega'(\bar{\lambda}_3)(2-s\bar{\lambda}_3)}{4+s^2} \\ G_0 &= \frac{1}{3} E_0^{\text{ux}} \end{aligned}$
Confined compression (cc)/ volumetric compression	$\begin{bmatrix} \lambda & 0 & 0 \\ 0 & 1 & 0 \\ 0 & 0 & 1 \end{bmatrix}$	$\begin{aligned} P_{xx} &= \frac{F_x}{A_x} \\ \sigma_{xx} &= P_{xx} \\ S_{xx} &= \frac{P_{xx}}{\lambda} \end{aligned}$	$\begin{aligned} \bar{I}_1 &= \lambda^{4/3} + \frac{2}{\lambda^{2/3}} \quad \bar{I}_2 = 2\lambda^{2/3} + \frac{1}{\lambda^{4/3}} \quad J = \lambda \\ P_{xx} &= \frac{4}{3} \left(\frac{\partial W}{\partial \bar{I}_1} + \frac{\partial W}{\partial \bar{I}_2} \frac{1}{\lambda^{2/3}} \right) \left(\lambda^{1/3} - \frac{1}{\lambda^{5/3}} \right) \\ &+ \frac{\partial W}{\partial J} \approx \frac{\partial W}{\partial J} \text{ if } \frac{\partial W}{\partial J} \gg \frac{\partial W}{\partial \bar{I}_1}, \frac{\partial W}{\partial \bar{I}_2} \\ M_0 &= \frac{4}{3} G_0 + K_0 \approx K_0 = \left(\frac{\partial^2 W}{\partial J^2} \right)_{J=1} \end{aligned}$	$\begin{aligned} \bar{\lambda}_1 &= \lambda^{2/3} \quad \bar{\lambda}_2 = \bar{\lambda}_3 = \frac{1}{\lambda^{1/3}} \quad J = \lambda \\ P_{xx} &= \frac{2}{3} (\omega'(\bar{\lambda}_1) \bar{\lambda}_1 - \omega'(\bar{\lambda}_3) \bar{\lambda}_3) \frac{1}{\lambda} \\ &+ \frac{\partial W}{\partial J} \approx \frac{\partial W}{\partial J} \text{ if } \frac{\partial W}{\partial J} \gg \omega' \\ M_0 &= \frac{4}{3} G_0 + K_0 \approx K_0 = \left(\frac{\partial^2 W}{\partial J^2} \right)_{J=1} \end{aligned}$

y-direction, the experimental stress obtained from the measured force F_x and the hyperelastic model response in each deformation mode.

Next, the simple shear test (ss) is introduced with the shear strain s , the deformation gradient

$$\mathbf{F} = \begin{bmatrix} 1 & s & 0 \\ 0 & 1 & 0 \\ 0 & 0 & 1 \end{bmatrix} = \underbrace{\begin{bmatrix} \frac{2}{\sqrt{s^2+4}} & \frac{s}{\sqrt{s^2+4}} & 0 \\ -\frac{s}{\sqrt{s^2+4}} & \frac{2}{\sqrt{s^2+4}} & 0 \\ 0 & 0 & 1 \end{bmatrix}}_{=\mathbf{R}} \cdot \underbrace{\begin{bmatrix} \frac{2}{\sqrt{s^2+4}} & \frac{s}{\sqrt{s^2+4}} & 0 \\ \frac{s}{\sqrt{s^2+4}} & \frac{s^2+2}{\sqrt{s^2+4}} & 0 \\ 0 & 0 & 1 \end{bmatrix}}_{=\mathbf{U}=\bar{\mathbf{U}}} \quad (26)$$

and $J = 1$.

Furthermore, the deformation gradient of the confined compression test (cc) reads

$$\mathbf{F} = \mathbf{U} = \begin{bmatrix} \lambda & 0 & 0 \\ 0 & 1 & 0 \\ 0 & 0 & 1 \end{bmatrix} = \underbrace{\begin{bmatrix} \lambda^{2/3} & 0 & 0 \\ 0 & 1/\lambda^{1/3} & 0 \\ 0 & 0 & 1/\lambda^{1/3} \end{bmatrix}}_{=\bar{\mathbf{U}}} J^{1/3} \quad \text{and} \quad \mathbf{R} = \mathbf{I} \quad (27)$$

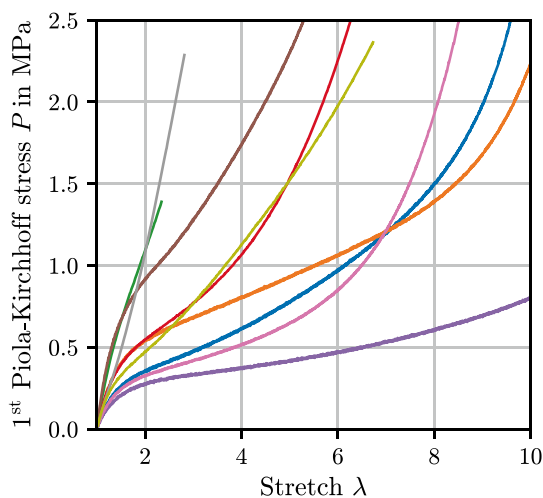
where $J = \lambda$. In case of nearly incompressible materials, $\sigma_{xx} \approx \sigma_{yy} = \sigma_{zz}$ can be observed, i.e., the deviatoric stress contribution σ_{iso} is negligible such that the approximation $\sigma \approx \sigma_{\text{vol}} = -p\mathbf{I}$ is valid. Thus, contrary to the biaxial tensile and simple shear tests which provide information about the isochoric response, the confined compression test reveals the volumetric behavior.

2.7 Experiments

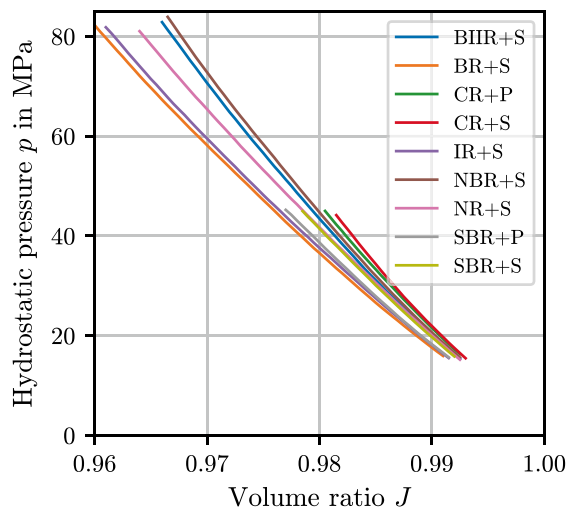
Experimental data of nine unfilled rubbers from quasi-static, uniaxial tensile tests as well as confined compression tests are employed, see Table 4, Fig. 1 and [84]. The uniaxial test data are used for the parameter identification of

Table 4 Recipes of the investigated rubbers (mass fractions are given in parts per hundred rubber)

Material	Type of rubber	Rubber	Sulfur (80 %)	Zinc oxide	Stearic acid	Peroxide
BIIR+S	Bromobutyl	100	2	5	2	
BR+S	Butadiene	100	2	5	2	
CR+P	Chloroprene	100				1.96
CR+S	Chloroprene	100	2	3	1	
IR+S	Isoprene	100	2	5	2	
NBR+S	Nitrile-butadiene	100	2	5	2	
NR+S	Natural rubber	100	2	5	2	
SBR+P	Styrene-butadiene	100				2.45
NBR+S	Styrene-butadiene	100	2	3	1	



(a) ux



(b) cc

Fig. 1 Experimental data from (a) uniaxial tensile and (b) confined compression tests with the rubber materials in Table 4 (data were processed according to procedures in Sect. 3.1 and 3.3, respectively; legend in (b) also applies to (a))

the \bar{I}_1 -dependent strain energy functions $W_{iso,1}$ in Sect. 4.2, whereas the volumetric strain energy functions W_{vol} are assessed with the data from confined compression tests in Sect. 5. All experiments were conducted with a Zwick 1445 universal test machine, cf. Supplementary Fig. 24(a). The tensile test procedure is based on the DIN 53504 standard (preload: 0.1 N; displacement rate: 200 mm/min; flat, shouldered specimen with 20 mm gauge length; optical strain measurement; loading until failure). For the confined compression tests, a tight-fitting, cylindrical specimen (diameter 7.5 mm; height 10 mm) is placed in the hole of a thick-walled metal cylinder. Thus, the lateral strain is suppressed when a compressive force is applied and a volume change is enforced. The data of both experiments are processed according to the procedures in Sect. 3.1 and 3.3, respectively, and afterwards resampled with equidistant strain

increments of 0.5 % (i.e., $\Delta\lambda = 0.005$) to ensure an equal weight of all strain regions in the fitting procedure.

Furthermore, the classical Treloar data set [95] comprised of uniaxial tension, pure shear and equibiaxial tension data of unfilled, sulfur-crosslinked natural rubber, cf. Fig. 2, is used for the discussions on \bar{I}_2 -dependent strain energy functions $W_{iso,2}$ in Sect. 4.3. It is processed according to Sect. 3.1 and its consistency is checked in Sect. 3.2. The choice of the Treloar data is explained by means of Supplementary Table 11 which lists frequently used experimental data sets for benchmarking constitutive models for rubbers (filled, thermoplastic and foamed elastomers are excluded since they cannot generally be idealized as volume preserving or free of dissipation and, hence, conflict with the model assumptions of perfect elasticity and incompressibility). First, it can be noticed that a lot of publications in the table provide general biaxial tension data sets rather than separate

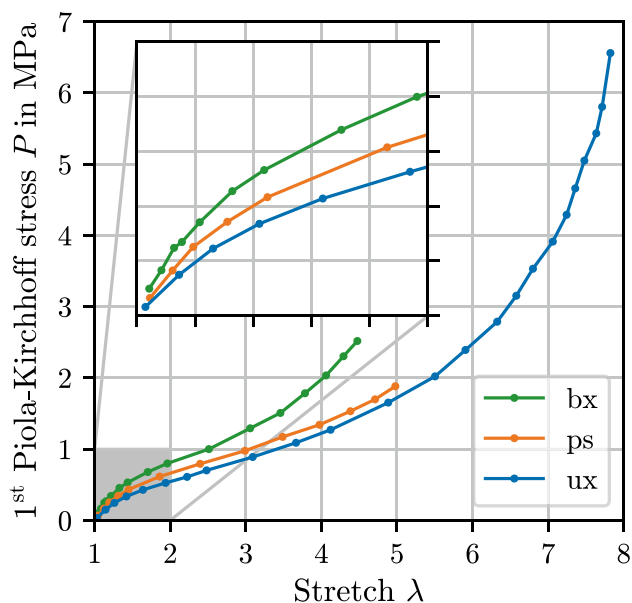


Fig. 2 Treloar data [95] with close-up of the small strain regime (data were processed according to procedure in Sect. 3.1; ux: uniaxial tension, ps: pure shear, bx: equibiaxial tension)

uniaxial, planar and equibiaxial tension data, cf. [52, 53, 56, 85, 98]. Such data require further discussions which are beyond the scope of this work, e.g., how to properly treat the second stress value P_{yy} in the cost function, see Sect. 2.8, or how to apply the data preparation and consistency check from Sect. 3. Moreover, the listed general biaxial tensile tests do not always cover the full range of biaxial deformation from uniaxial ($\lambda_2 = 1/\sqrt{\lambda_1}$) to equibiaxial tension ($\lambda_2 = \lambda_1$) at all λ_1 -levels, cf. [53, 85, 98], or the maximum stretch is comparatively small. The remaining references often lack in detailed information about the experimental procedure or present incomplete data sets, i.e., the uniaxial, planar or equibiaxial tensile test is missing, cf. [1, 3, 104]. In addition, as nearly all data sets in the table are based on similar natural rubber compounds with comparable properties, the evaluation of several of these sets would lead to redundant findings. Due to the outlined considerations, the probably most frequently used and well established Treloar data are considered here, see for example [11, 13, 16, 36, 57, 58, 63, 67, 73] or Table 1. Although his measurement methods are outdated and he did not table the test data, Treloar [95] explained in detail his experimental setups and findings. Moreover, he presented interesting discussions on the systematic error in pure shear experiments, the equivalence of equibiaxial tension and uniaxial compression and the need of sample preconditioning by comparing the loading and unloading curves. Nevertheless, extensive, complete and consistent data sets for several rubber compounds from a modern test machine and up to large stretches with an analysis of error sources are still missing in the literature.

2.8 Parameter Fitting

Parameter fitting (also known as model calibration or parameter identification) is an optimization procedure which searches for the best parameter set of a material model such that the difference between the model response and given experimental data is minimal in a certain sense. Here, the p -norm of the residual array is minimized leading to the cost function

$$F_k(\rho_1, \dots, \rho_n) = \left(\frac{1}{m_k} \sum_{i=1}^{m_k} |r_i|^p \right)^{1/p} \rightarrow \min \quad (28)$$

with the residual of the i -th data point (of experiment k with m_k data points)

$$\begin{aligned} k = ux, ps, bx, cc : \quad r_i &= P_{xx,mod}(\lambda_{exp,i}, \rho_1, \dots, \rho_n) - P_{exp,xx,i} \\ k = ss : \quad r_i &= P_{xy,mod}(s_{exp,i}, \rho_1, \dots, \rho_n) - P_{exp,xy,i} \end{aligned} \quad (29)$$

where ρ_j , $j = 1, \dots, n$ are the material parameters. $\lambda_{exp,i}$ and $P_{exp,xx,i}$ are the measured stretch and 1st Piola-Kirchhoff stress in direction of tension/compression and $s_{exp,i}$ and $P_{exp,xy,i}$ are the measured shear strain and stress. The model response $P_{mod,xx,i}$ or $P_{mod,xy,i}$ is computed according to Table 3. Common choices for the norm order are $p = 1$ (taxicab norm), $p = 2$ (Euclidean norm) or $p = \infty$ (maximum norm), i.e., the mean error, the root mean square error (RMSE) or the maximum error are minimized. When multiple experiments are fitted simultaneously, the cost function is given by $F = \sum_k F_k$. In this case, the factor $1/m_k$ in Eq. (28) eliminates a weighting of the experiments due to different numbers of data points.

The residual in Eq. (29) is defined in terms of the absolute error of the 1st Piola-Kirchhoff stress. Other reasonable error types are the relative error

$$r_i = \frac{P_{mod} - P_{exp,i}}{P_{exp,i}} \quad (30)$$

or the normalized error

$$r_i = \frac{P_{mod} - P_{exp,i}}{\max |P_{exp,i}|} \quad (31)$$

where the indices xx or xy are omitted for the sake of a more general notation. These two residuals scale the error from each experiment in order to eliminate a weighting when multiple experiments with different stress ranges are fitted, see for example the Treloar data in Fig. 2 with a maximum uniaxial stress of 6.6 MPa and a maximum equibiaxial stress of 2.5 MPa. In addition, the relative error in residual (30) gives a higher weight to the range of low stresses than the

absolute and normalized error but may generate dubious r_i when dividing by noisy stress values $P_{exp,i}$ close to zero.

An alternative formulation of the cost function is obtained by replacing the 1st Piola-Kirchhoff stress \mathbf{P} by the Cauchy stress $\boldsymbol{\sigma}$. For the biaxial tensile tests (ux, ps and bx), this is equivalent to multiplying the residual by $\lambda_{exp,i} > 1$, cf. Table 3. Thus, it amplifies deviations from large stresses. Vice versa, replacing \mathbf{P} by the 2nd Piola-Kirchhoff stress \mathbf{S} leads to a division by $\lambda_{exp,i}$ for these deformation modes and, hence, errors at small stress are more penalized. For simple shear, the 1st Piola-Kirchhoff stress is identical to the Cauchy stress $P_{xy} = \sigma_{xy}$. Whereas the 2nd Piola-Kirchhoff stress obtained from $S_{xy} = P_{xy} - sP_{yy}$ is experimentally not accessible since the stress component P_{yy} is usually not measured². For confined compression, the 1st Piola-Kirchhoff stress is equal to the Cauchy stress, too, whereas the 2nd Piola-Kirchhoff stress scales \mathbf{P} by $1/\lambda_{exp,i}$. In Sect. 4.1.3, the effects of the norm order, stress measure and error type on the fitting result are illustrated so that a reasonable choice for the subsequent studies and model comparisons can be made.

For the parameter identification, the SciPy optimize library is used. The implementation of the hyperelastic models is done with the Mathematica Add-On AceGen, cf. [62]. More precisely, the strain energy function is programmed in the symbolic Wolfram language such that the stresses as well as the exact Jacobian, i.e., derivative of the stress w.r.t. the material parameters are obtained via automatic differentiation. Then, AceGen generates numerically efficient Fortran or C subroutines which are callable within the SciPy algorithms, e.g., via the F2PY tool of the NumPy library.

3 Data Preparation

3.1 Preload Correction in Tensile Tests

For tensile tests with flat specimens, a small preload is typically applied to ensure a plane, non-buckling reference configuration. Moreover, it avoids difficulties for the controller of the test machine when encountering such a possibly unstable load state. The preload is ideally chosen as small as possible while it concurrently guarantees a straightened specimen. This balance may depend on the material's stiffness, the test machine settings and the specimen clamping, e.g., for different loading modes. Thus, no universal, best

choice exists. Possible preload correction procedures are discussed below.

Since the preload leads to a slight stress offset of the first data point, many test machines provide an option to zero the load cell after applying the preload. As a consequence, the whole stress-strain curve is shifted along the stress-axis such that the first data point provides zero stress at zero strain. This procedure (hereinafter referred to as initial stress correction or vertical shifting) is not ideal since the preload is actually present and should not be ignored. To overcome this drawback, an alternative to the stress correction is provided. Let us assume that the testing machine measures optically the distance in loading direction between two reference points on the specimen rather than the displacement of the traverse. The measured length in the current state at time t_i and in the preloaded reference state are denoted by ℓ_i and ℓ_0^* , respectively, leading to the erroneous stretch $\lambda_i^* = \ell_i/\ell_0^*$. Hence, the initial length ℓ_0^* must be corrected because the elongation due to the preload, i.e., the prestretch $\lambda_{pre} = \ell_0^*/\ell_0$ with the true initial length ℓ_0 is not captured by the testing machine. This correction does not lead to a shifting of the stress-axis but to a scaling of the stretch-axis by λ_{pre} , viz., the true stretch is obtained by

$$\lambda_i = \lambda_i^* \lambda_{pre} = \frac{\ell_i}{\ell_0^*} \frac{\ell_0^*}{\ell_0} = \frac{\ell_i}{\ell_0} \tag{32}$$

Therefore, this procedure is referred to as initial stretch correction or horizontal scaling. In the following, a procedure to find a good approximation of λ_{pre} is proposed:

1. Extract the data at small strains. The exact range must be checked for each material and deformation mode. For the materials depicted in Fig. 1(a), $1 < \lambda < 1.1$ is a good overall choice.
2. Choose an appropriate strain energy function which is able to reproduce the small strain behavior well. For the unfilled rubbers in Fig. 1(a), a Neo-Hooke approach $W_{iso} = c_{10}(\bar{I}_1 - 3)$ is sufficient³.
3. Fit the chosen strain energy function to the extracted data with a modified stretch input according to Eq. (32). That is, $\lambda_i = \lambda_i^* \lambda_{pre}$ where λ_i^* are the measured stretches and λ_{pre} is the prestretch which is treated as an additional fitting parameter. If data sets from multiple deformation modes are available, this fitting should be done for each experiment separately.
4. Scale all measured stretches λ_i^* by the fitted prestretch λ_{pre} to obtain the corrected stretches: $\lambda_i = \lambda_i^* \lambda_{pre}$.

² Note that a simple shear deformation state $\mathbf{F} = \mathbf{I} + s \mathbf{e}_x \otimes \mathbf{e}_y$ is assumed here which generally does not lead to a simple shear stress state $\boldsymbol{\sigma} = \sigma_{xy}(\mathbf{e}_x \otimes \mathbf{e}_y + \mathbf{e}_y \otimes \mathbf{e}_x)$, i.e., $\sigma_{xx} = \sigma_{yy} = \sigma_{zz} = 0$ for finite strains, see for instance [93].

³ For highly filled rubbers with a high initial stiffness and pronounced softening at small strains, an exponential $A/B(1 - \exp(-B(\bar{I}_1 - 3)))$ or a logarithmic term $A/B \ln(1 + B(\bar{I}_1 - 3))$ can be added.

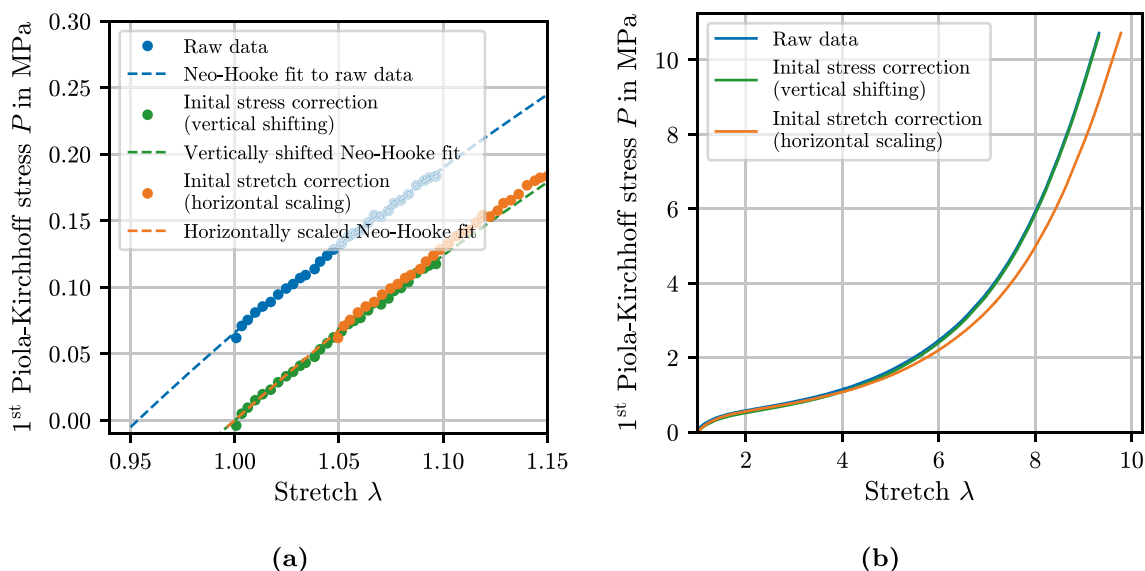


Fig. 3 Procedure of the proposed initial stretch correction for the CR+S compound: **(a)** The Neo-Hooke model with the modified stretch input according to Eq. (32) is fitted to the raw data (blue); The additional fitting parameter λ_{pre} is used to scale the stretch data (orange); For illustration, the conventional initial stress correction

which shifts the data vertically, viz., zeroing the load cell after applying the preload is depicted as well (green). **(b)** Effect of the initial stretch as well as initial stress correction on the whole data range (the fitted parameters are $\lambda_{\text{pre}} = 1.051$, $c_{10} = 0.225$)

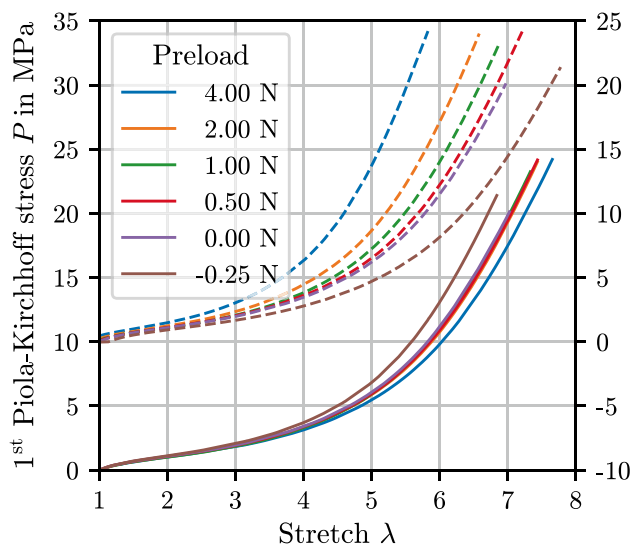


Fig. 4 Proposed initial stretch correction applied to tensile tests with the same material but different preloads: The raw data are plotted as dashed lines and, for the sake of readability, with an offset of 10 MPa, cf. right axis, whereas the corrected data are given as solid lines

The proposed procedure is applied to all compounds in Fig. 1(a), see Table 6 for the fitted shear moduli $G_0 = 2c_{10}$. It is illustrated for the CR+S compound in Fig. 3(a). The fitted value $\lambda_{\text{pre}} = 1.051$ states that the specimen of this compound was prestretched by 5.1 % due to the preload. The effect of the initial stretch correction is compared to the

initial stress correction in Fig. 3(b). The difference between both approaches is pronounced particularly at large strains.

Furthermore, Fig. 4 depicts the effect of the initial stretch correction on the stress-stretch curves of uniaxial tensile tests with the same material but different preloads from -0.25 N (i.e., a buckled specimen with an underestimated initial length) to 4 N (i.e., a strongly prestretched specimen with an overestimated initial length). It can be observed that the corrected curves nearly coincide over a large range of preloads. Only the stress responses with the negative and highest preload deviate slightly at large strains. In contrast, the stress correction is not able to reasonably compensate the preload dependency as it would lead to a shift of all data points by only $-0.03 \dots 0.5$ MPa ($-0.25 \dots 4$ N on a cross section area of approx. 2×4 mm²). The effect would be barely visible in the stress-stretch plot. Thus, the presented initial stretch correction should be preferred. However, the choice of the applied preload is still to be made carefully and depends on several factors as outlined at the beginning of this section. In general, negative and very large preloads should be avoided.

3.2 Consistency Check of Tensile and Shear Tests

Experimental data obtained from uniaxial tensile tests are very reliable and reproducible. In contrast, pure shear, equibiaxial tension and simple shear measurements require more difficult, error-prone setups which do not yield exactly the desired deformation states. For instance, the pure shear state

Table 5 Initial moduli of the Treloar data [95]

Deformation mode	Initial modulus	Ratio to E_0^{ux}	Theoretical ratio to E_0^{ux}	Ratio to E_0^{ps}	Theoretical ratio to E_0^{ps}	Prestretch λ_{pre}
ux	$E_0^{ux} = 1.165$ MPa					1.027
ps	$E_0^{ps} = 1.605$ MPa	1.378	1.333			1.008
bx	$E_0^{bx} = 2.481$ MPa	2.131	2	1.546	1.5	1.008

is commonly obtained from a tensile test using a specimen with a high aspect ratio (width to length), cf. Supplementary Fig. 24(b). The high aspect ratio minimizes the lateral contraction but, nevertheless, leads to a non-homogeneous deformation at the edges. Moreover, this setup requires highly parallel and concentric lower and upper clamping as well as specimens with a constant thickness over the specimen width. In case of equibiaxial tensile tests with a clamping frame as shown in Supplementary Fig. 24(c), the friction between the clamps and the rails causes an overstiff response. Note also that the simple shear deformation given in Eq. (26) is just an idealization of the real distortion, especially for large strains.

Due to the variety of errors, experimental data can readily be inconsistent, i.e., the measured response from different deformation modes do not comply with theoretical considerations. For invariant- or stretch-based hyperelastic models under the assumption of incompressibility, the ratios between the initial tangent moduli are fixed and independent of the chosen strain energy function:

- Use the identified parameters of the strain energy function to compute the initial moduli according to Eq. (33).
- Prove that $E_0^{ps}/E_0^{ux} \approx 4/3$, $E_0^{bx}/E_0^{ux} \approx 2$ and $G_0^{ss}/E_0^{ux} \approx 1/3$.

For illustration, this procedure is applied to the Treloar data in Fig. 2 considering the Neo-Hooke model and the strain range $1 < \lambda < 1.35$. The fitted initial moduli and prestretches are given in Table 5. Both, the initial modulus of the pure shear data as well as the equibiaxial data are slightly too stiff but still in good agreement with the uniaxial Young’s modulus. Thus, reasonable results can be expected when fitting hyperelastic models under the assumption of incompressibility.

3.3 Data Processing of Confined Compression Tests

Confined compression tests typically show a too compliant (33)

$$\begin{aligned}
 E_0^{ux} &= \lim_{\lambda \rightarrow 1} \frac{dP_{xx}^{ux}}{d\lambda} = 6 \left(\frac{\partial W}{\partial \bar{I}_1} + \frac{\partial W}{\partial \bar{I}_2} \right)_{\substack{\bar{I}_1=3 \\ \bar{I}_2=3}} = \frac{3}{2} (\omega'(1) + \omega''(1)) \\
 E_0^{ps} &= \lim_{\lambda \rightarrow 1} \frac{dP_{xx}^{ps}}{d\lambda} = 8 \left(\frac{\partial W}{\partial \bar{I}_1} + \frac{\partial W}{\partial \bar{I}_2} \right)_{\substack{\bar{I}_1=3 \\ \bar{I}_2=3}} = 2(\omega'(1) + \omega''(1)) = \frac{4}{3} E_0^{ux} \\
 E_0^{bx} &= \lim_{\lambda \rightarrow 1} \frac{dP_{xx}^{bx}}{d\lambda} = 12 \left(\frac{\partial W}{\partial \bar{I}_1} + \frac{\partial W}{\partial \bar{I}_2} \right)_{\substack{\bar{I}_1=3 \\ \bar{I}_2=3}} = 3(\omega'(1) + \omega''(1)) = 2 E_0^{ux} \\
 G_0^{ss} &= \lim_{s \rightarrow 1} \frac{dP_{xy}^{ss}}{ds} = 2 \left(\frac{\partial W}{\partial \bar{I}_1} + \frac{\partial W}{\partial \bar{I}_2} \right)_{\substack{\bar{I}_1=3 \\ \bar{I}_2=3}} = \frac{1}{2} (\omega'(1) + \omega''(1)) = \frac{1}{3} E_0^{ux}
 \end{aligned}$$

If the experimental data do not exhibit these ratios, no model would be able to reproduce the behavior properly. Therefore, it is advisable to check the consistency before running the model calibration:

- Run the initial stretch correction from Sect. 3.1 for each experiment. If an initial stretch correction is not desired or needed, run the procedure anyway but keep the pre-stretch constant $\lambda_{pre} = 1$, i.e., the strain energy function is fitted to the unmodified data.

behavior at small deformations because the sample diameter is slightly less than the bore diameter of the specimen holder. When the pressure is applied, the material can expand a bit in lateral direction such that initially the response is predominantly isochoric. Once the nearly incompressible rubber comes into contact with the inner surface of the specimen holder, the stress response increases notably due to the much stiffer volumetric behavior. Unfortunately, this stress upturn is smooth rather than abrupt. Hence, the challenge is to find a point that represents this transition in order to approximate the specimen height h_0 when the volumetric

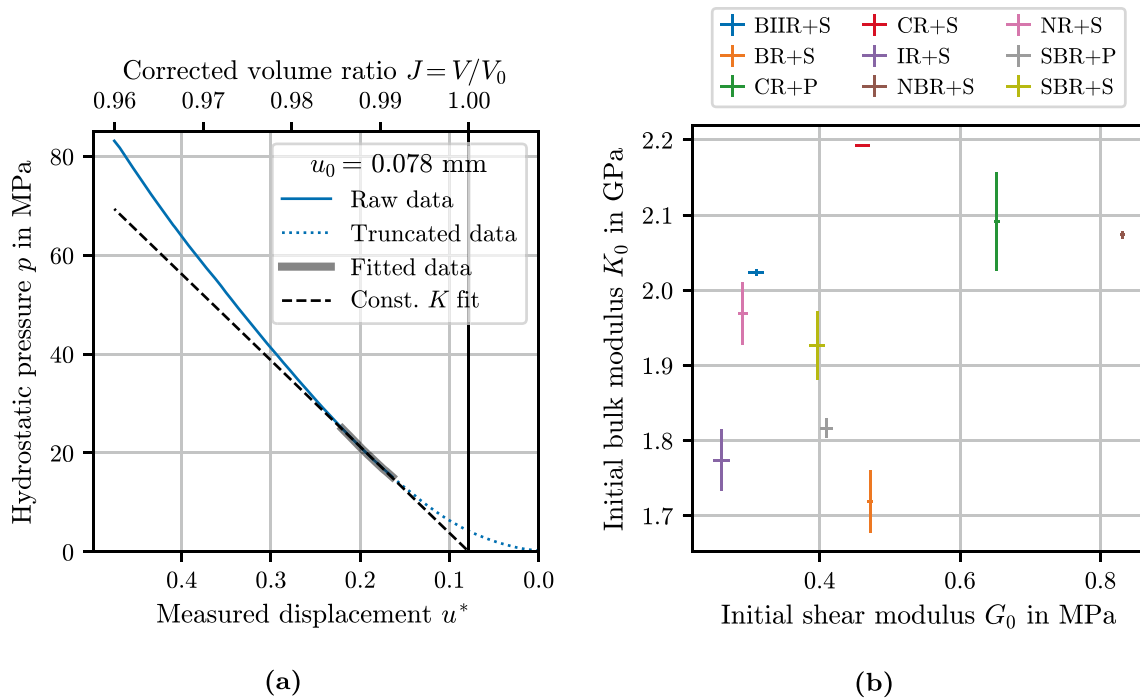


Fig. 5 (a) Proposed data processing for confined compression tests applied to the IR+S compound: the linear p - J -model with the modified input according to Eq. (34) is fitted to the data range between 15

and 25 MPa; (b) initial shear and bulk moduli according to the procedures in Sect. 3.1 and 3.3, respectively (the + represents moduli from two uniaxial tensile tests as well as two confined compression tests)

Table 6 Initial shear moduli G_0 and bulk moduli K_0 according to the procedures in Sect. 3.1 and 3.3, respectively, as well as Poisson ratios obtained by $\nu_0 = (3 K_0/G_0 - 2)/(6 K_0/G_0 + 2)$ and measured mass

	BIIR+S	BR+S	CR+P	CR+S	IR+S	NBR+S	NR+S	SBR+P	NBR+S
G_0 in MPa	0.309	0.472	0.652	0.461	0.260	0.831	0.291	0.410	0.397
K_0 in GPa	2.023	1.719	2.091	2.192	1.774	2.074	1.969	1.816	1.926
$\nu_0 = 0.499 \dots$	$\dots 924$	$\dots 863$	$\dots 844$	$\dots 895$	$\dots 927$	$\dots 800$	$\dots 926$	$\dots 887$	$\dots 897$
ρ_0 in g/mm ³	0.960	0.946	1.256	1.273	0.941	1.014	0.949	0.946	0.970

densities ρ_0 of the rubbers in Fig. 1 (all values are the average of two measurements)

deformation begins. A suitable approach is proposed below and exemplified in Fig. 5(a) using the IR+S compound. The crucial differences to the preload correction in Sect. 3.1 are: it is presumed that the applied preload is negligibly small, the height of the undeformed specimen h_0^* is known and the displacement is measured rather than the strain.

1. Choose a lower pressure bound (e.g., 15 MPa in Fig. 5(a)) above which the response can be definitely assumed to be volumetric and truncate the data below.
2. Choose an upper bound up to which the volumetric response is approximately linear (e.g., 25 MPa).
3. Fit the model $p = -K_0(J - 1)$ to this pressure range with the constant bulk modulus K_0 and a modified input

Table 7 Isochoric strain energy functions depending on the first invariant (an asterisk * indicates models that were originally defined in terms of the first as well as second invariant or principal stretches and are reduced by replacing $\bar{I}_2 \rightarrow 3$ or $\bar{\lambda}_i \rightarrow 1$; n is the number of parameters and the imposed parameter restrictions)

No.	Name	Literature	Strain energy function $W_{iso,1}$	n
0	Neo-Hooke	[99] Eq. (10)	$c_{10}(\bar{I}_1 - 3)$	1
1*	Isihara	[51] Eq. (25)	$c_{10}(\bar{I}_1 - 3) + c_{20}(\bar{I}_1 - 3)^2$	2
2	Knowles	[61] Eq. (4.1)	$\frac{G_0}{2b} \left(\left(\frac{b}{n}(\bar{I}_1 - 3) + 1 \right)^n - 1 \right)$	2
3	Kilian	[59] Eq. (17)	$G_0 \left(-(\bar{I}_m - 3)(\ln(1 - \eta) + \eta) - \frac{2}{3}a \left(\frac{\bar{I}_1 - 3}{2} \right)^{3/2} \right), \eta = \sqrt{\frac{\bar{I}_1 - 3}{\bar{I}_m - 3}}$	3 ($\bar{I}_m > 3$)
4*	Swanson	[92] Eq. (13)	$\frac{3}{2} \sum_{i=1}^m \frac{A_i}{\alpha_i} \left((\bar{I}_1/3)^{\alpha_i} - 1 \right), m = 2$	4
5*	Edwards & Vilgis	[29] Eq. (4.31)	$\frac{G_c}{2} \frac{(1-\alpha)\bar{I}_1}{1-\alpha\bar{I}_1} + \ln(1 - \alpha\bar{I}_1)$	2 ($0 < \alpha < 1/3$)
6	bin Othman & Gregory	[12] Eq. (10)	$\frac{A}{2}(\bar{I}_1 - 3) - \frac{C}{B^2} \log \left(\frac{B}{C} \sqrt{\bar{I}_1 - 3} + 1 \right) + \frac{1}{B} \sqrt{\bar{I}_1 - 3}$	3
7	Yeoh	[102] Eq. (10)	$c_{10}(\bar{I}_1 - 3) + c_{20}(\bar{I}_1 - 3)^2 + c_{30}(\bar{I}_1 - 3)^3$	3
8*	Yamashita & Kawabata	[101] Eq. (16)	$c_{10}(\bar{I}_1 - 3) + \frac{A}{\alpha}(\bar{I}_1 - 3)^\alpha$	3 ($\alpha \geq 1$)
9	extended Yeoh	[103] Eq. (20)	$c_{10}(\bar{I}_1 - 3) + c_{20}(\bar{I}_1 - 3)^2 + c_{30}(\bar{I}_1 - 3)^3 + \frac{A}{B}(1 - \exp(-B(\bar{I}_1 - 3)))$	5
10	Arruda & Boyce	[3] Eq. (15) with series expansion Eq. (21)	$G \left(\frac{1}{2}(\bar{I}_1 - 3) + \frac{1}{20N}(\bar{I}_1^2 - 9) + \frac{11}{1050N^2}(\bar{I}_1^3 - 27) + \frac{11}{1050N^2}(\bar{I}_1^3 - 27) + \frac{19}{7000N^3}(\bar{I}_1^4 - 81) + \frac{519}{673750N^4}(\bar{I}_1^5 - 243) \right)$	2
11	8-chain	[3] Eq. (15) with approx. by [19] Eq. (10)	$G \left(\frac{1}{6}(\bar{I}_1 - 3) - \frac{\bar{I}_m}{3} \ln \left(1 - \frac{\bar{I}_1 - 3}{\bar{I}_m - 3} \right) \right)$	2 ($\bar{I}_m > 3$)
12	Davies	[23] Eq. (22)	$\frac{G}{2(1-\alpha)} \left((\bar{I}_1 - 3 + C)^{1-\alpha} - C^{1-\alpha} \right) + k(\bar{I}_1 - 3)^2$	4
13	Gent	[31] Eq. (3)	$-\frac{G_0}{2}(\bar{I}_m - 3) \ln \left(1 - \frac{\bar{I}_1 - 3}{\bar{I}_m - 3} \right)$	2 ($\bar{I}_m > 3$)
14*	Lion	[65] Eq. (4.8a)	$c_{10}(\bar{I}_1 - 3) + c_{50}(\bar{I}_1 - 3)^5$	2
15*	Yeoh & Fleming	[104] Eq. (24)	$\frac{A}{B}(1 - \exp(-B(\bar{I}_1 - 3))) - c_{10}(\bar{I}_m - 3) \ln \left(1 - \frac{\bar{I}_1 - 3}{\bar{I}_m - 3} \right)$	4 ($\bar{I}_m > 3$)

$$J_i = 1 - \frac{u_i}{h_0} = 1 - \frac{u_i^* - u_0}{h_0^* - u_0} \tag{34}$$

where u_i^* and u_i are the measured and corrected displacement at time t_i . Note that the displacement is defined to be positive in compression direction. u_0 is the applied displacement, i.e., the height reduction when the specimen comes into contact with the inner surface of the specimen holder and the volumetric deformation begins. It is considered as an additional fitting parameter besides K_0 .

- Use the identified u_0 to derive the volume change from the measured displacement: $J_i = 1 - (u_i^* - u_0)/(h_0^* - u_0)$

The preload correction is applied to all confined compression tests from Fig. 1(b), see Table 6 for the fitted bulk moduli K_0 . Moreover, the K_0 values are plotted against the shear moduli G_0 from Sect. 3.1 in Fig. 5(b). No correlation between the bulk modulus, shear modulus, Poisson ratio or mass density can be observed. However, the provided initial shear and bulk moduli may serve as a data source for future numerical work lacking in experimental data and, hence, realistic parameter values.

Table 8 Cont.: Isochoric strain energy functions depending on the first invariant (an asterisk * indicates models that were originally defined in terms of the first as well as second invariant or principal stretches and are reduced by replacing $\bar{I}_2 \rightarrow 3$ or $\bar{\lambda}_i \rightarrow 1$; n is the number of parameters and the imposed parameter restrictions; comments on specific models: 17) further terms are omitted since they cannot be represented in terms of elementary functions, 22) $\alpha_1 = 1$ is fixed to ensure a non-zero initial modulus)

No.	Name	Literature	Strain energy function $W_{iso,1}$	n
16	Gregory	[35], cf. [94] Eq. (13)	$\frac{A}{2(1-\alpha)} \left((\bar{I}_1 - 3 + C)^{1-\alpha} - C^{1-\alpha} \right) + \frac{B}{2(1+\beta)} \left((\bar{I}_1 - 3 + C)^{1+\beta} - C^{1+\beta} \right)$	5
17*	Lambert-Diani & Rey	[63] Eq. (25)	$\frac{\exp(a_0)}{a_1} \left(\exp(a_1(\bar{I}_1 - 3)) - 1 \right)$	2
18*	extended tube	[54] Eq. (50)	$\frac{G_c}{2} \frac{(1-1/n)(\bar{I}_1-3)}{1-(\bar{I}_1-3)/n} + \ln\left(1 - \frac{\bar{I}_1-3}{n}\right)$	2 ($n>0$)
19	Boyce & Arruda	[13] Eq. (27)	$\frac{3}{2} \sum_{i=1}^m \frac{\Delta_i}{i} \left((\bar{I}_1/3)^i - 1 \right), \quad m = 4$	4
20*	Haupt & Sedlan	[40] Eq. (62)	$c_{10}(\bar{I}_1 - 3) + c_{30}(\bar{I}_1 - 3)^3$	2
21*	Hartmann & Neff	[38] Eq. (3.4)	$\alpha(\bar{I}_1^3 - 27) + c_{10}(\bar{I}_1 - 3)$	2
22*	Beda	[10] Eq. (27)	$\sum_{i=1}^m \frac{\Delta_i}{\alpha_i} (\bar{I}_1 - 3)^{\alpha_i} \quad \alpha_1 = 1, m = 2$	3 ($\alpha_i \geq 1$)
23	Lim	[64] Eq. (69)	$\frac{G_1}{2} (\bar{I}_1 - 3) - \frac{G_2}{2} (\bar{I}_m - 3) \ln\left(1 - \frac{\bar{I}_1-3}{\bar{I}_m-3}\right)$	3 ($\bar{I}_m > 3$)
24	Beatty	[8] Eq. (7.2)	$-\frac{G_0 \bar{I}_m (\bar{I}_m - 3)}{2(2\bar{I}_m - 3)} \ln\left(\frac{1-(\bar{I}_1-3)/(\bar{I}_m-3)}{1+(\bar{I}_1-3)/\bar{I}_m}\right)$	2 ($\bar{I}_m > 3$)
25	Hoss & Marczak	[47] Eq. (3)	$\frac{A}{2a} (1 - \exp(-a(\bar{I}_1 - 3))) + \frac{B}{2b} \left(\left(\frac{b}{n}(\bar{I}_1 - 3) + 1 \right)^n - 1 \right)$	5
26*	Carroll	[16] Eq. (19)	$\frac{3}{2} \left(A(\bar{I}_1/3 - 1) + \frac{B}{4} \left((\bar{I}_1/3)^4 - 1 \right) \right)$	2
27	Dobrynin & Carrillo	[25] Eq. (1)	$\frac{G}{2} \left((\bar{I}_1 - 3) + \frac{6(\bar{I}_1-3)}{(\beta-1)(\beta\bar{I}_1-3)} \right)$	2 ($0 < \beta < 1$)
28	Khajehsaeid	[57] Eq. (19)	$\frac{G_0}{2} \left(\frac{1}{a} (\exp(a(\bar{I}_1 - 3)) - 1) + b((\bar{I}_1 - 2)(1 - \ln(\bar{I}_1 - 2)) - 1) \right)$	3
29*	Network averaging tube	[58] Eq. (25)	$\mu_{ck} n \ln\left(\frac{\sin(\pi/\sqrt{n})(\bar{I}_1/3)^{q/2}}{\sin(\pi/\sqrt{n})(\bar{I}_1/3)^{q/2}}\right)$	3 ($q > 0, n > 1$)
30*	Xiang	[100] Eq. (22)	$G_c n \ln\left(\frac{3n+\bar{I}_1/2}{3n-\bar{I}_1}\right)$	2 ($n > 1$)
31*	Zhao	[105] Eq. (17)	$A_{21}(\bar{I}_1 - 3) + A_{41}(\bar{I}_1^2 - 9) + A_{42}(\bar{I}_1^2 - 9)^2$	3
32*	simplified tube	[81] Eq. (5)	$\frac{G_c}{2} \frac{\bar{I}_1-3}{1-(\bar{I}_1-3)/n}$	2 ($n > 0$)
33	Fu	[30] Eqs. (10)–(11)	$G \left(\frac{1}{2}(\bar{I}_1 - 3) + \frac{1}{20N}(\bar{I}_1^2 - 9) + \frac{11}{1050N^2}(\bar{I}_1^3 - 27) + \frac{19}{7000N^3}(\bar{I}_1^4 - 81) + \frac{519}{673750N^4}(\bar{I}_1^5 - 243) \right) + \frac{a}{b} (\exp(b(\bar{I}_1 - 3)) - 1)$	4

4 Fitting of Isochoric Strain Energy Functions

4.1 Preliminaries

4.1.1 Fitting Procedure, Considered Models and Parameter Limits

The fitting procedure for the isochoric strain energy is divided into two parts. At first, the uniaxial tension data of the nine rubbers depicted in Fig. 1(a) are used to identify promising \bar{I}_1 -dependent strain energy functions for each

compound. Thereafter, the best performing \bar{I}_1 -based models are combined with several \bar{I}_2 -terms and fitted simultaneously to the uniaxial tension, pure shear and equibiaxial tension data of the natural rubber from Treloar [95]. This separated procedure is followed to systematically investigate the role of both terms. In particular, the relevance of the second invariant is pointed out and conclusions for reliable parameter identifications are drawn, see Sect. 4.1.2. Before presenting the fitting results for the \bar{I}_1 - and \bar{I}_2 -terms in Sect. 4.2 and 4.3, respectively, the chosen residual formulation is discussed and illustrated in Sect. 4.1.3.

Table 9 Isochoric strain energy functions depending on the second invariant (all models were originally defined in terms of both the first and second invariant and are reduced by replacing $\bar{I}_1 \rightarrow 3$; n is the number of material parameters and the imposed parameter restrictions; comments on specific models: 4) the linear term is omitted to obtain a two-parameter model, 6) further terms are omitted since they cannot be represented in terms of elementary functions)

No.	Name	Literature	Strain energy function $W_{iso,2}$	n
0	No \bar{I}_2 -dependency	–	0	0
1	Mooney-Rivlin	[76] Eq. (14)	$c_{01}(\bar{I}_2 - 3)$	1
2	Gent & Thomas	[32] Eq. (3)	$\frac{3G_2}{2} \ln(\bar{I}_2/3)$	1
3	Klingbeil & Shield	[60] Eqs. (4.1), (4.3) & (4.7)	$\frac{3G_2}{2m} ((\bar{I}_2/3)^m - 1)$	2
4	Alexander	[1] Eq. (52)	$\frac{G_2\gamma}{2} \ln((\bar{I}_2 - 3)/\gamma + 1)$	2
5	Haines & Wilson	[36] Eq. (2.1)	$c_{01}(\bar{I}_2 - 3) + c_{02}(\bar{I}_2 - 3)^2$	2
6	Lambert-Diani & Rey	[63] Eq. (25)	$\frac{G_2}{2m} (\bar{I}_2 - 3)^m$	2 ($m \geq 1$)
7	Chevalier & Marco	[18] Eq. (13)	$c_{01}(\bar{I}_2 - 3) + \frac{3G_2}{2} \ln(\bar{I}_2/3)$	2
8	Pucci & Saccomandi	[82] Eq. (32)	$-\frac{G_2}{2} (\bar{I}_m - 3) \ln\left(1 - \frac{\bar{I}_2 - 3}{\bar{I}_m - 3}\right)$	2 ($\bar{I}_m > 3$)
9	Hartmann & Neff	[38] Eq. (3.4)	$c_{01}(\bar{I}_2^{3/2} - 3^{3/2})$	1
10	Carroll	[16] Eq. (19)	$3G_2\left(\sqrt{\bar{I}_2/3} - 1\right)$	1
11	Mansouri & Darijani	[67] Eq. (14)	$\frac{G_2}{2a} (\exp(a(\bar{I}_2 - 3)) - 1)$	2
12	Dal	[21] Eqs. (34) ₂ & (35) ₂	$\frac{9}{2} G_2\left(\sqrt[3]{\bar{I}_2/3} - 1\right)$	1

The considered strain energy functions of this study are collected from the literature and compiled in Tables 7, 8 and 9. Note that for models depending on both invariants \bar{I}_1 and \bar{I}_2 one of them is formally set equal to 3 to obtain separated formulations (in a similar manner, possible stretch-based terms are eliminated by setting all $\bar{\lambda}_k = 1$). That is, some models differ from their original formulation (indicated by an asterisk * in the tables) and approaches with coupled terms are beyond the scope of this work. All strain energy functions are proven to satisfy the following requirements:

- For \bar{I}_1 - and \bar{I}_2 -based strain energy functions, the maximum number of parameters is five and two, respectively.
- A closed-form representation of the strain energy in terms of elementary functions must be available. In addition, models requiring numerical integration, internal iterations or other computationally costly aspects are excluded as well.
- Only models that are particularly developed for rubbers are considered. For instance, some publications consider also models for isotropic soft tissues. However, due to the characteristic tension-compression asymmetry of tissues (i.e., the stress response is more pronounced under compression than under tension), different modeling approaches are necessary, see also [75, 15].

The fitting is conducted with the following parameter restrictions:

- The initial shear modulus G_0 , cf. Eq. (33), must be finite (e.g., for the term $(\bar{I}_1 - 3)^\alpha$, this requirement is fulfilled for $\alpha \geq 1$)
- For limited stretch models, i.e., models with a pole, the singularity is ensured to appear at $\bar{I}_1 > 3, \bar{I}_2 > 3$ (e.g., this implies $\bar{I}_m > 3$ for the term $-\ln(1 - (\bar{I}_1 - 3)/(\bar{I}_m - 3))$).

All remaining material parameters can assume any real number. Indeed, these requirements are very generous and may lead to numerically undesirable or physically implausible behavior for arbitrary deformation states. However, finding suitable parameter bounds for each strain energy function is not reasonable for a large number of models. It depends on the imposed restrictions, cf. Sect. 2.4, and often leads to an optimization problem subjected to additional constraints. Moreover, promising models can easily be overlooked due to too strong constraints. Especially, when combining \bar{I}_1 - and \bar{I}_2 -models, parameter limits are often too restrictive, e.g., demanding convexity for both $W_{iso,1}$ and $W_{iso,2}$. Therefore, the results are proven after the fitting to fulfill monotonicity conditions, viz., the Cauchy stress as well as the 1st Piola-Kirchhoff stress increase monotonically in the experimental strain range. A stability check beyond the maximum strain of the considered data is not taken into account since the specimens are loaded until failure. Any discussion on a physical plausible behavior beyond the elongation at break is pointless and, for numerical stability, an extrapolation with a constant modulus can be implemented.

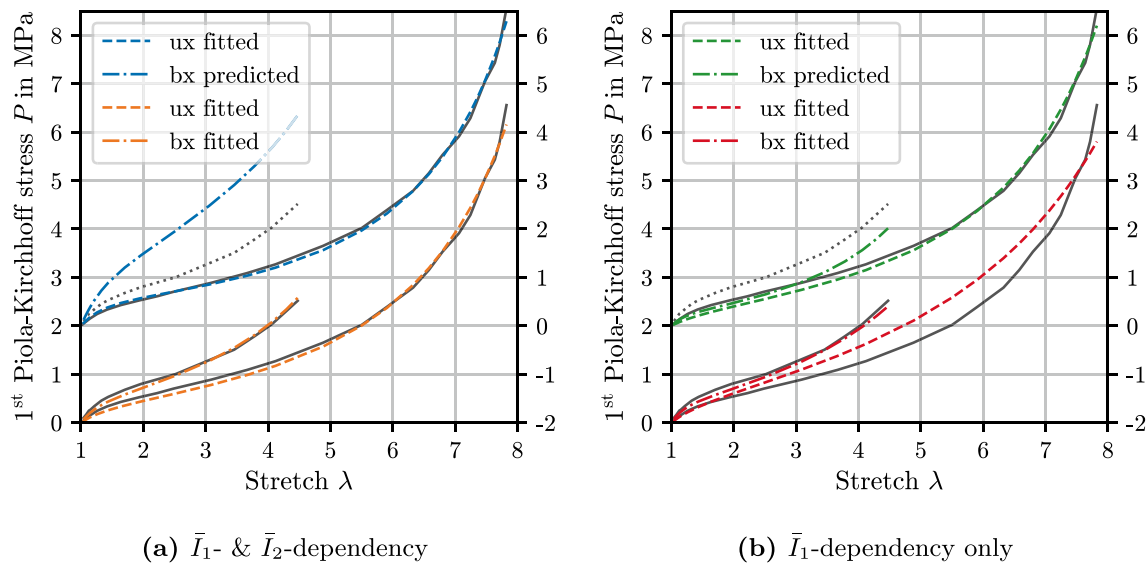


Fig. 6 (Grey lines) Uniaxial (ux) and equibiaxial (bx) data from Treloar [95]; (orange lines) the simplified tube model, cf. Eq. (35), is fitted simultaneously to ux and bx data; (blue lines) the model is fitted only to the ux data and predicts the response to the bx deformation;

(red lines) the simplified tube model without the \bar{I}_2 -term is fitted simultaneously to ux and bx data; (green lines) the model without the \bar{I}_2 -term is fitted only to the ux data and predicts the response to the bx deformation

Demanding monotonicity of the Cauchy stress is a fundamental, physically motivated requirement and equivalent to satisfying the Baker-Ericksen inequalities $(\sigma_i - \sigma_j)(\lambda_i - \lambda_j) > 0$ for $i \neq j$. Whereas monotonicity of the 1st Piola-Kirchhoff stress is a necessary condition to ensure a stable material behavior in the sense of Hill and Drucker [44, 28]. That is, the incremental work defined by $\Delta \mathbf{F} \cdot \Delta \mathbf{u}$ must be positive where $\Delta \mathbf{u}$ is the displacement increment due to the additional external force $\Delta \mathbf{F}$. For the biaxial deformation states, it is equivalent to $\Delta P_{xx} \Delta \lambda > 0$ and for simple shear to $\Delta P_{xy} \Delta s > 0$. Note that monotonicity of the 1st Piola-Kirchhoff stress implies monotonicity of the Cauchy stress.

4.1.2 Role of the Second Principal Invariant

Many hyperelastic material models are defined in terms of the first principal invariant \bar{I}_1 or in terms of the first and second principal invariant \bar{I}_1 and \bar{I}_2 , see for instance [20] for an overview. The additional dependency on \bar{I}_2 , its physical meaning and its role within the fitting procedure are discussed by many authors. A comprehensive review on experimental findings was given by Kawabata & Kawai [55]. Assuming incompressibility, they discussed the stress dependency (more precisely, the derivatives $\partial W / \partial \bar{I}_1$ and $\partial W / \partial \bar{I}_2$) for biaxial deformation modes within the small as well as large strain regime and at different temperatures. Also the relaxation behavior, the effect of filler and different polymers were investigated. In context of construction and calibration of strain energy functions, two important

outcomes are: $\partial W / \partial \bar{I}_1 > \partial W / \partial \bar{I}_2$ holds true for all deformations and $\partial W / \partial \bar{I}_2$ can take negative values at small strains. Under the assumption of a simple network, Kawabata & Kawai [55] derived a micromechanical interpretation of their observations stating that the \bar{I}_1 -dependency is „related primarily to intramolecular forces“ while the \bar{I}_2 -dependency is „a manifestation of intermolecular interactions“. However, it can be noticed that physically motivated modeling approaches rarely result in a strain energy function in terms of the second principal invariant. For instance, so-called tube models are typically comprised of a crosslink part defined in terms of \bar{I}_1 and a stretch-based part accounting additionally for chain entanglements, cf. [29, 42].

Destrade et al. [24] discussed the \bar{I}_2 -dependency based on observations from systematic fittings. They stated that „the \bar{I}_2 -dependence is precisely the missing ingredient to obtain excellent agreement in the small-to-moderate regime“ when fitting the Mooney-Rivlin model to uniaxial tension of the Treloar data. Indeed, the stress-strain curve is well fitted in the considered strain regime and deformation mode. However, their parameters lead to $c_{10} < c_{01}$, i.e., $\partial W / \partial \bar{I}_1 < \partial W / \partial \bar{I}_2$ what is contrary to the experimental findings explained above. Moreover, these parameters result in an overstiff response under equibiaxial tension.

The authors of the present manuscript are of the opinion that the ratio between the \bar{I}_1 - and \bar{I}_2 -dependency, i.e., $\partial W / \partial \bar{I}_1$ and $\partial W / \partial \bar{I}_2$ is essential to balance the model response in different deformation modes. This interpretation is motivated by the dependence of the stress response on \bar{I}_2 for each

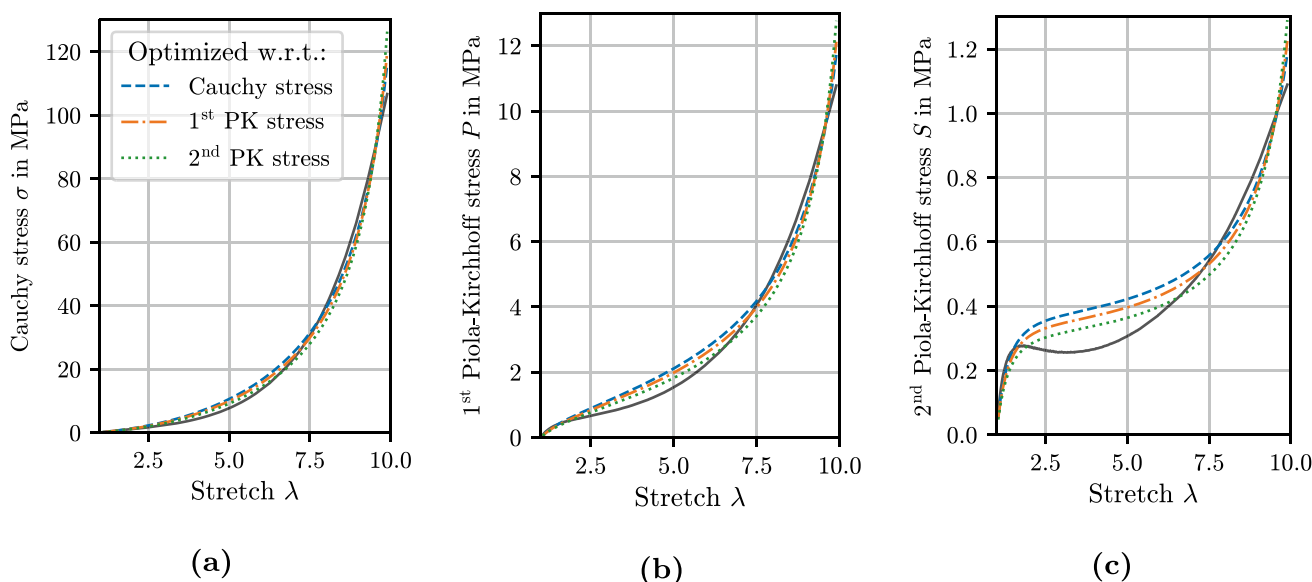


Fig. 7 Effect of the stress measure in the cost function on the fitting result: all three figures show the same data using different stress measures (a) Cauchy stress, (b) 1st Piola-Kirchhoff stress, (c)

2nd Piola-Kirchhoff stress (the black solid lines are the experimental data from the CR+S compound; PK: Piola-Kirchhoff)

deformation mode in Table 3. On the one hand, compared to the $\partial W/\partial \bar{I}_1$ -contribution, the $\partial W/\partial \bar{I}_2$ -term in the constitutive equation is scaled by $1/\lambda < 1$ for uniaxial tension and by $\lambda^2 > 1$ for equibiaxial tension, whereas the $\partial W/\partial \bar{I}_1$ - and $\partial W/\partial \bar{I}_2$ -term are weighted equally for simple and pure shear. On the other hand, it should be noted that for these four deformation modes \bar{I}_1 and \bar{I}_2 are not independent of each other, see App. C for the $\bar{I}_2(\bar{I}_1)$ -dependencies. In particular, the relations $\bar{I}_1 > \bar{I}_2$ for uniaxial tension, $\bar{I}_1 < \bar{I}_2$ for equibiaxial tension and $\bar{I}_1 = \bar{I}_2$ for simple as well as pure shear can be shown. That is, uniaxial tension is primarily driven by \bar{I}_1 and equibiaxial tension by \bar{I}_2 whereas the shear deformations are equally affected by both invariants. As a consequence of this predetermined weighting between the \bar{I}_1 - and \bar{I}_2 -contribution in different deformation modes, test data from only one experiment is insufficient for the calibration of models with \bar{I}_1 - and \bar{I}_2 -dependency because a plausible extrapolation to other deformation modes cannot be guaranteed.

This conclusion should not be taken as a drawback of invariant-based models compared with stretch-based models. In fact, leaving out the \bar{I}_2 -dependency when fitting to only one deformation mode is a possibility to avoid unforeseen behavior in the other deformation modes. In contrast, there is no straightforward method for stretch-based models to ensure in advance a reasonable behavior for other deformation modes. This is due to the fact that both terms $\omega'(\bar{\lambda}_1)$ and $\omega'(\bar{\lambda}_3)$ always appear in the constitutive equations, cf. Table 3.

To illustrate the considerations regarding the \bar{I}_2 -dependency, the simplified tube model by [81]

$$W_{\text{iso}}(\bar{I}_1, \bar{I}_2) = \frac{G_c}{2} \frac{\bar{I}_1 - 3}{1 - \frac{\bar{I}_1 - 3}{n}} + 3 G_e \left(\sqrt{\frac{\bar{I}_2}{3}} - 1 \right) \quad (35)$$

is employed with G_c , G_e and n being the crosslink modulus, entanglement modulus and elastically active chain length, respectively. It depends on both principal invariants and is

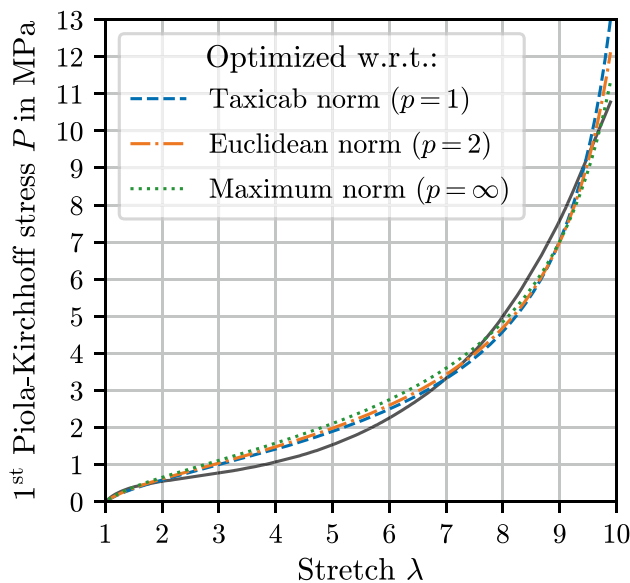


Fig. 8 Effect of the norm order p in the cost function on the fitting result (the black solid line is the experimental data from the CR+S compound)

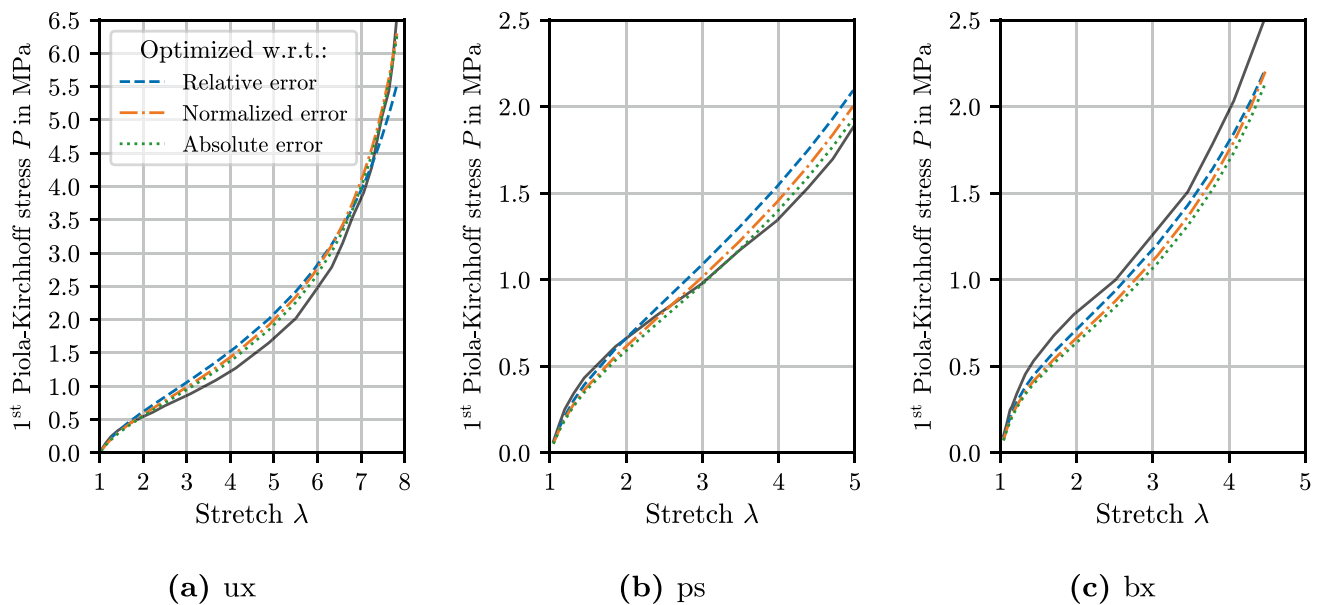


Fig. 9 Effect of the error type in the cost function on the fitting result (the black solid lines are the experimental data from Treloar [95])

calibrated on the Treloar data (with an Euclidean norm, normalized error, 1st Piola-Kirchhoff stress) in four different ways, see Fig. 6. First, the model is fitted to the uniaxial as well as equibiaxial data. Then, only the uniaxial data are considered for the parameter identification and the calibrated model is used to predict the equibiaxial response. Afterwards, this procedure is repeated with $G_e = 0$ such that the \bar{I}_2 -dependency is turned off. It can be observed that the model with \bar{I}_2 -dependency is generally able to fit the uniaxial and equibiaxial data very well. When the equibiaxial data are not considered for the model calibration, the uniaxial fit at small strains ($\lambda < 4$) improves. However, the equibiaxial response is drastically overestimated. In contrast, the model without \bar{I}_2 -dependency cannot capture both deformation modes simultaneously since the ratio between the model's response under uniaxial tension and equibiaxial tension is fixed and does not match with the experimental data. Thereby, the equibiaxial prediction is less random and still acceptable compared to the prediction with both \bar{I}_1 - and \bar{I}_2 -dependency. A similar finding was described by Seibert & Schöche [88] who attest "pure \bar{I}_1 -dependent formulations [...] the best predictive properties of multiaxial deformation states when the material parameters were determined on the basis of uniaxial data" only. Also Boyce & Arruda [13] studied the predictive capability of hyperelastic models and observed that "strain energy expressions which contain the second invariant [...], \bar{I}_2 , should be used with caution; forms such as the Mooney-Rivlin model are found to be overly stiff in certain types of deformation".

4.1.3 Effect of the Stress Measure, Norm Order and Error Type in the Cost Function

As mentioned in Sect. 2.8, there are several ways to define the cost function for the fitting procedure. To illustrate the effect of different stress measures and norm orders, the 8-chain model by [3] with the inverse Langevin function approximation by [19] is fitted to the data of the CR+S compound. Furthermore, to illustrate the influence of the error types, the Treloar data [95] are employed.

Fig. 7 shows the influence of the stress measure on the fitting result. As explained in Sect. 2.8, different stress measures emphasize different sections of the stress-strain curve. The optimization w.r.t. the Cauchy stress leads to the smallest deviations at large stretches ($\lambda > 7.5$) whereas the 2nd Piola-Kirchhoff stress provides the smallest errors in the range $1.75 < \lambda < 6.5$. The 1st Piola-Kirchhoff stress is a tradeoff with a stress-strain curve in between. Note that this and the following effects can be more or less pronounced depending on the experimental data and the model capability, e.g., a perfectly fitting model would be unaffected by the definition of the cost function.

In Fig. 8, the order of the p -norm in the cost function Eq. (28) is varied. The taxicab norm with $p = 1$ optimizes the mean absolute error, i.e., high deviations at large strains can be compensated by a good fit at low strains. In contrast, the maximum norm ($p = \infty$) takes only the maximum error of the whole strain range into account. As a consequence, the deviations of the stress response at very large stretches ($\lambda > 9.5$) are much lower in exchange for a worsened fit at $\lambda < 7$. The result with the Euclidean norm ($p = 2$) is a

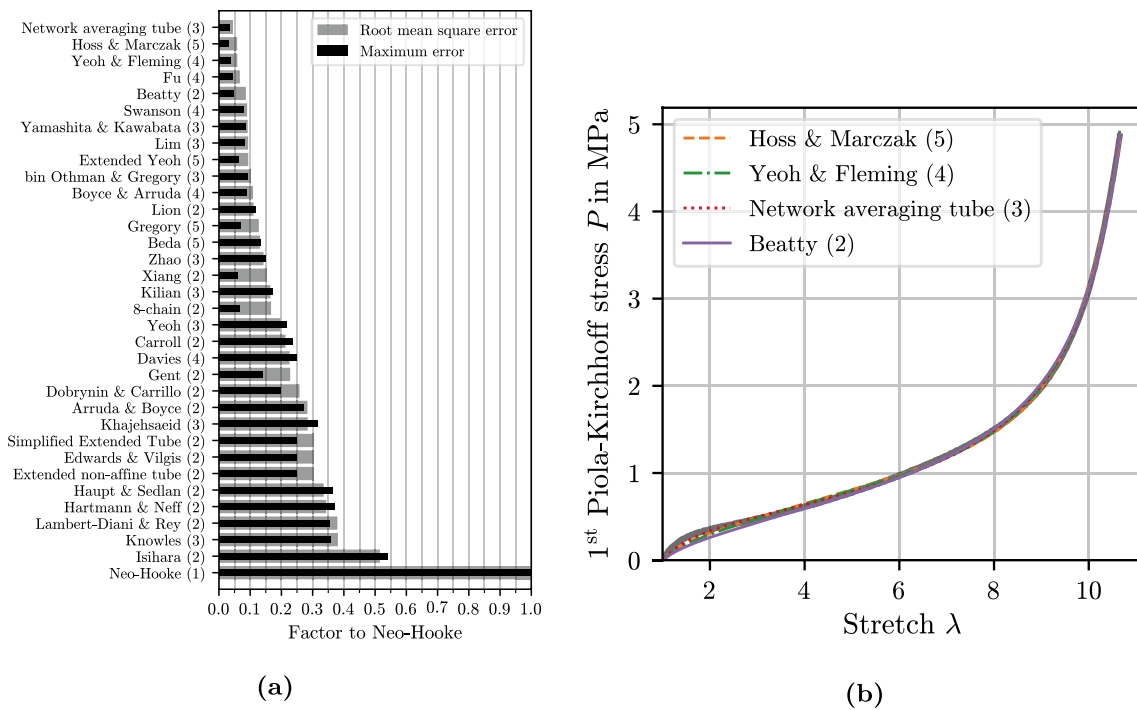


Fig. 10 Fitting results for the BIIR+S compound: (a) ranking sorted by RMSE, (b) stress-stretch curve of the best performing models with five, four, three and two parameters (experimental data are shown as grey, solid line; number of parameters is given in brackets)

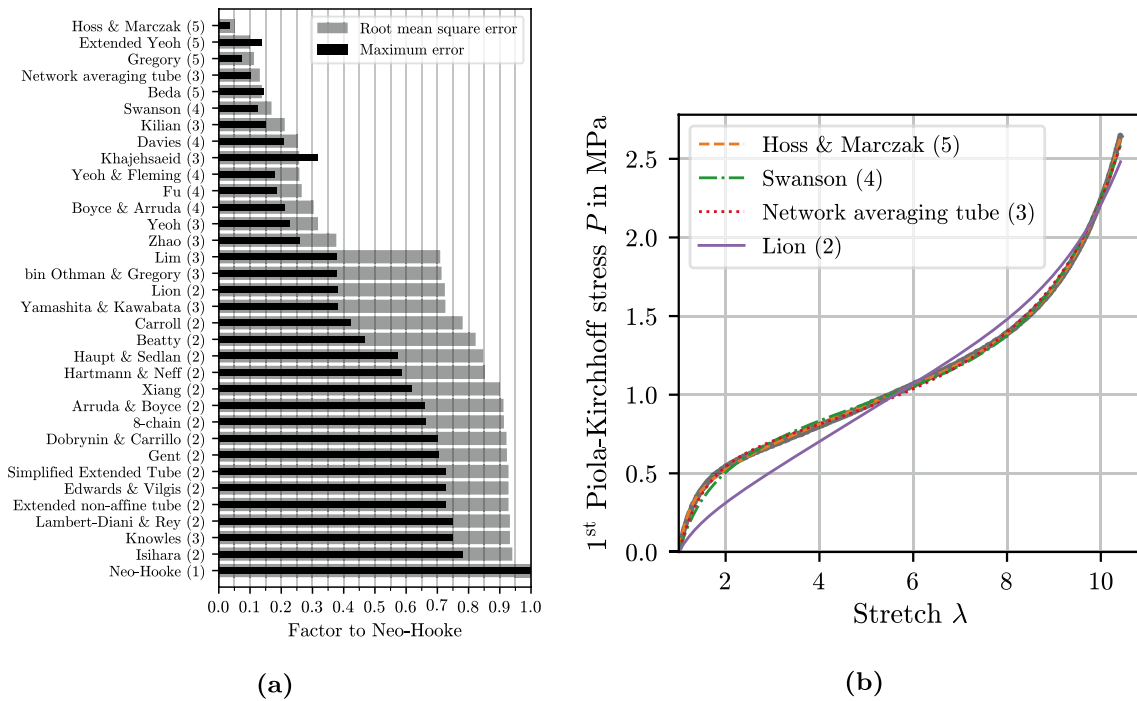
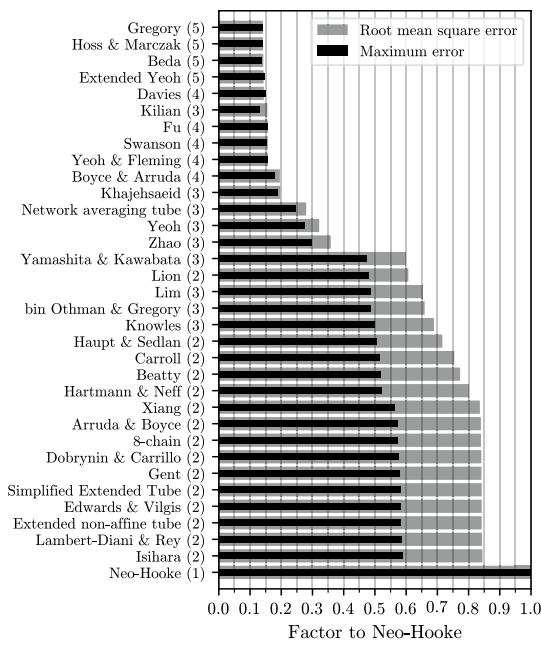
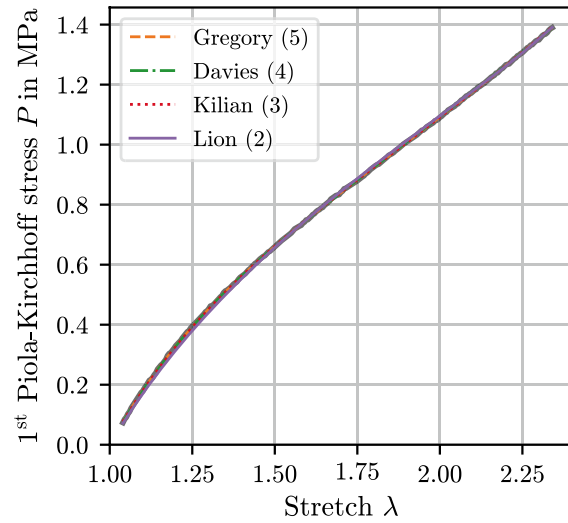


Fig. 11 Fitting results for the BR+S compound: (a) ranking sorted by RMSE, (b) stress-stretch curve of the best performing models with five, four, three and two parameters (experimental data are shown as grey, solid line; number of parameters is given in brackets)

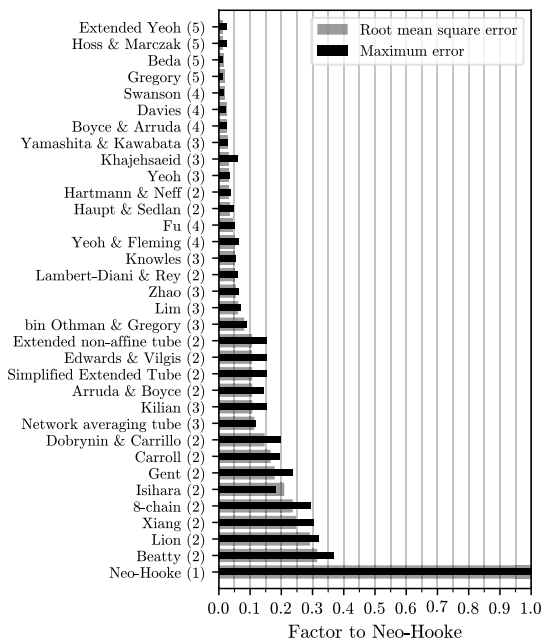


(a)

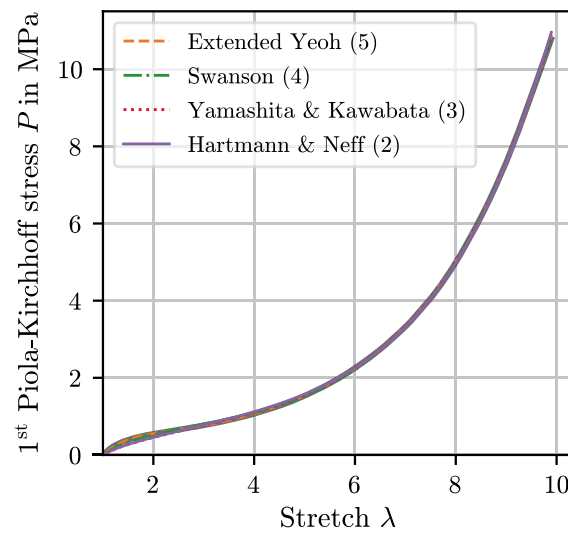


(b)

Fig. 12 Fitting results for the CR+P compound: (a) ranking sorted by RMSE, (b) stress-stretch curve of the best performing models with five, four, three and two parameters (experimental data are shown as grey, solid line; number of parameters is given in brackets)



(a)



(b)

Fig. 13 Fitting results for the CR+S compound: (a) ranking sorted by RMSE, (b) stress-stretch curve of the best performing models with five, four, three and two parameters (experimental data are shown as grey, solid line; number of parameters is given in brackets)

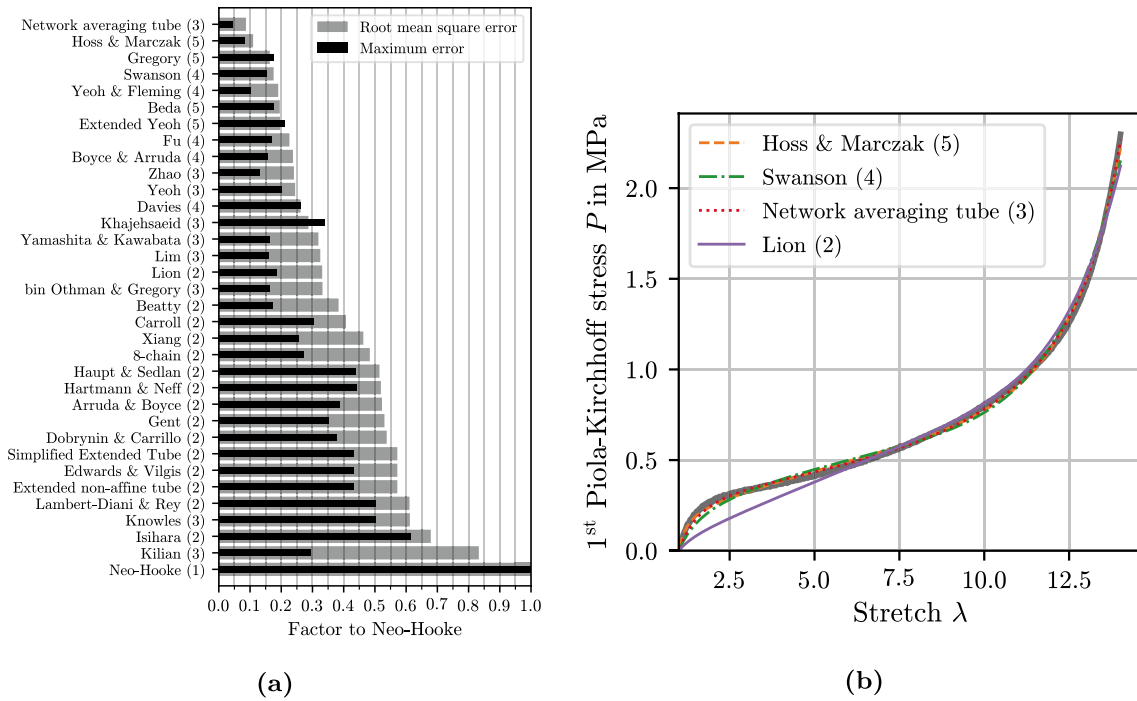


Fig. 14 Fitting results for the IR+S compound: (a) ranking sorted by RMSE, (b) stress-stretch curve of the best performing models with five, four, three and two parameters (experimental data are shown as grey, solid line; number of parameters is given in brackets)

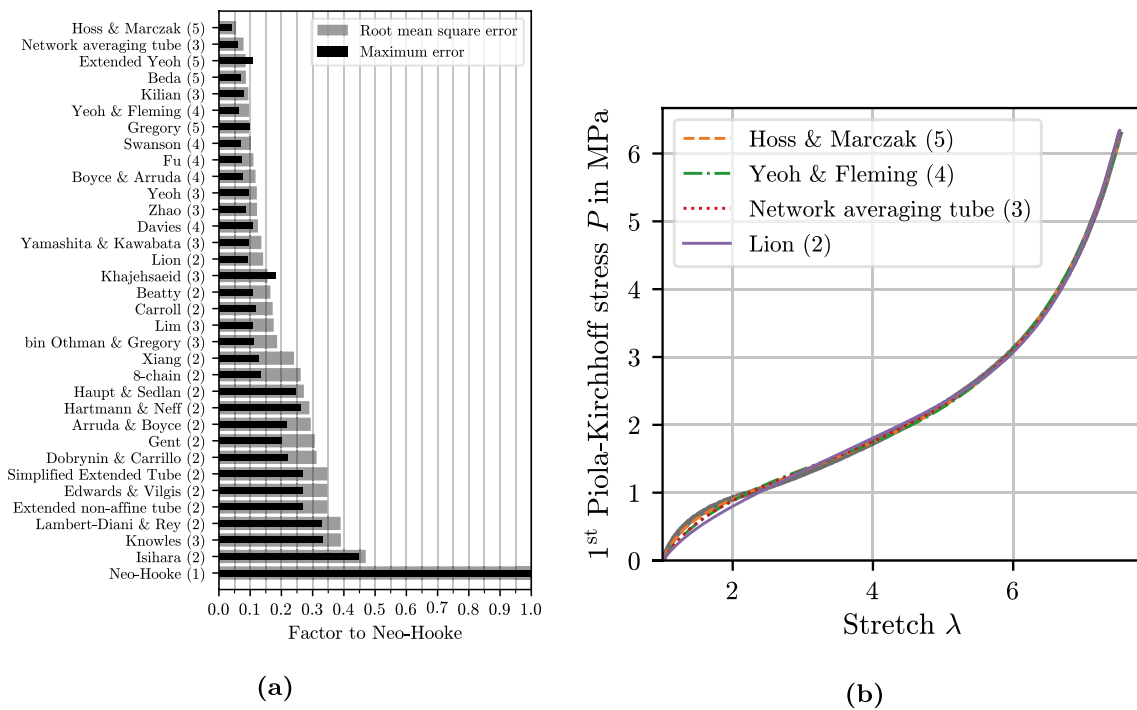


Fig. 15 Fitting results for the NBR+S compound: (a) ranking sorted by RMSE, (b) stress-stretch curve of the best performing models with five, four, three and two parameters (experimental data are shown as grey, solid line; number of parameters is given in brackets)

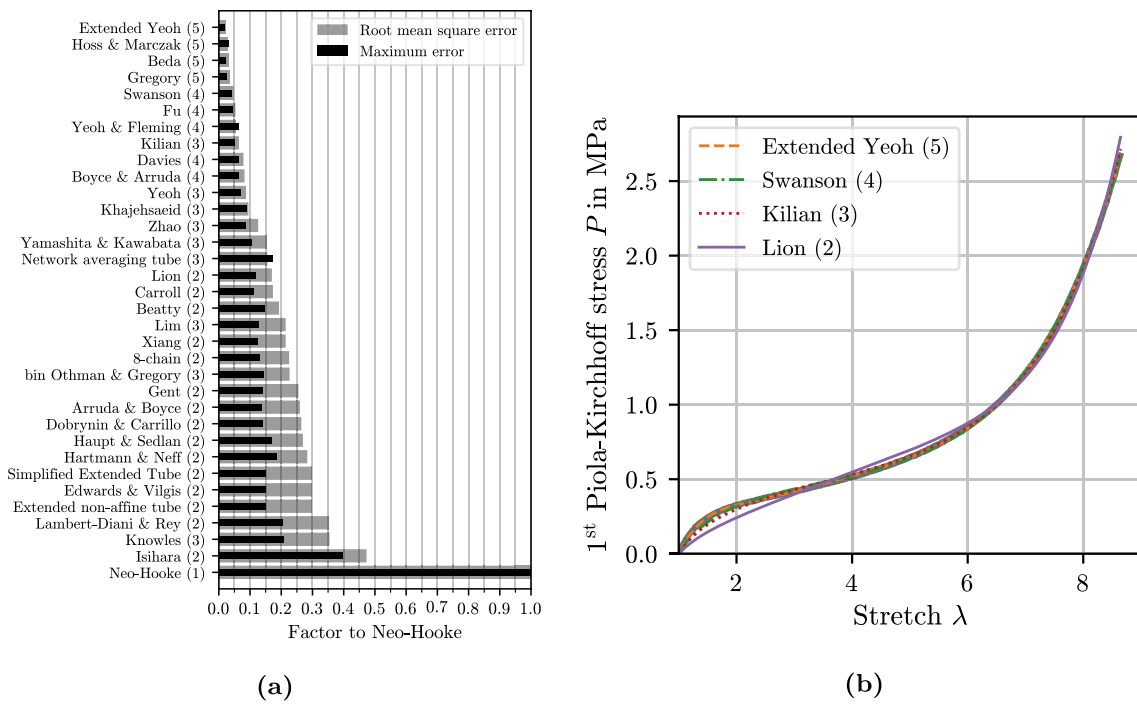


Fig. 16 Fitting results for the NR+S compound: (a) ranking sorted by RMSE, (b) stress-stretch curve of the best performing models with five, four, three and two parameters (experimental data are shown as grey, solid line; number of parameters is given in brackets)

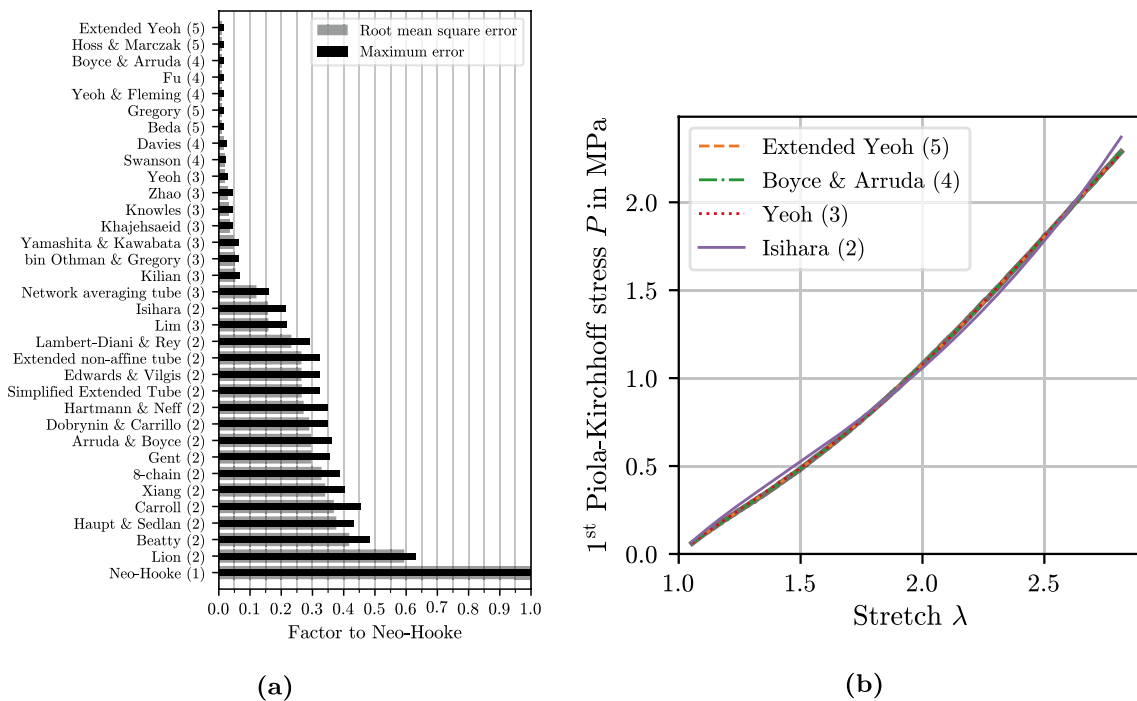


Fig. 17 Fitting results for the SBR+P compound: (a) ranking sorted by RMSE, (b) stress-stretch curve of the best performing models with five, four, three and two parameters (experimental data are shown as grey, solid line; number of parameters is given in brackets)

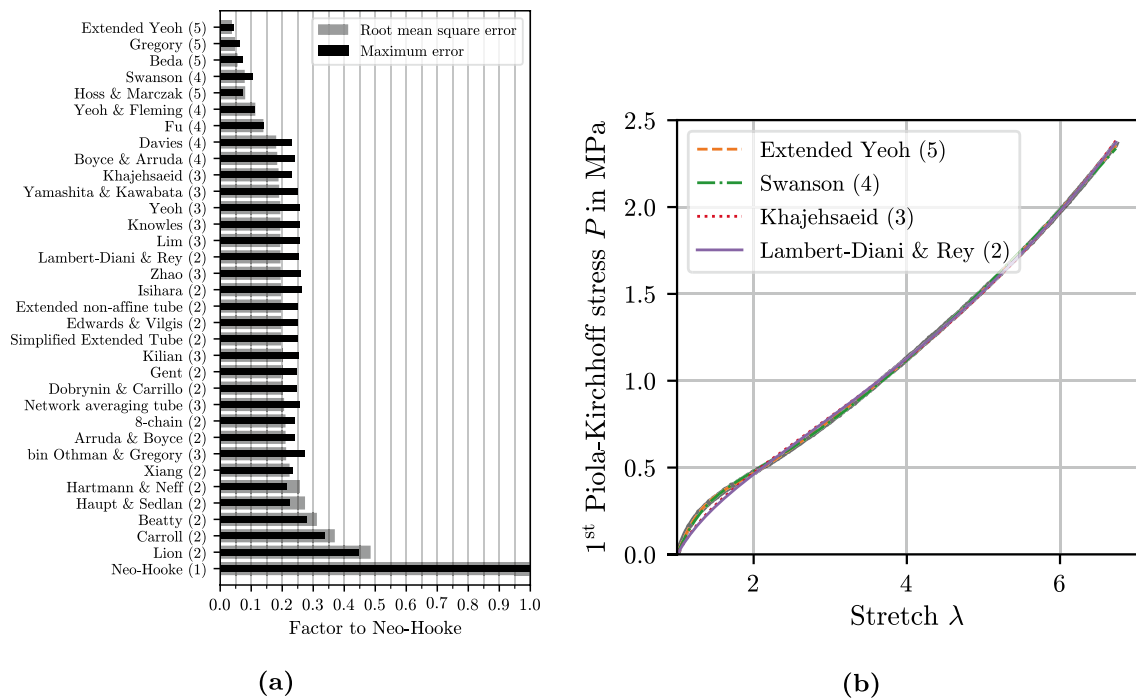


Fig. 18 Fitting results for the SBR+S compound: **(a)** ranking sorted by RMSE, **(b)** stress-stretch curve of the best performing models with five, four, three and two parameters (experimental data are shown as grey, solid line; number of parameters is given in brackets)

compromise with a slight bias towards the result obtained with $p = 1$.

Finally, the effect of the error type in the residual is shown in Fig. 9. Here, the 8-chain model is simultaneously fitted to all three deformation modes of the Treloar data using an absolute, normalized and relative error, cf. Eqs. (29)–(31). In general, it can be observed that the chosen model is not able to capture the stress response of the three experiments simultaneously, see also Sect. 4.1.2. More specific, the uniaxial response tends to be overestimated and the equibiaxial response underestimated. Using an absolute error, the fit to the uniaxial tensile test is slightly better than for the other error types, especially for $\lambda > 2$, but at the expense of the goodness of fit to the equibiaxial data. Vice versa, the relative error leads to better results for the equibiaxial experiment but worse results for the uniaxial one, see explanation in Sect. 2.8. Moreover, it improves the results for small strains ($\lambda < 1.5$) of all deformation modes. The result obtained with the normalized error lies in between the other results. Note that, if one compares the effect of the error type by means of only one experiment, the absolute error and normalized error would coincide.

In summary, the formulation of the cost function has an essential influence on the rankings in the subsequent sections. Therefore, this choice must be made carefully. In the present manuscript, the

- Euclidean norm
- Normalized error
- 1st Piola-Kirchhoff stress

are preferred and employed in all parameter optimizations and numerical investigations due to the following reasons. The Euclidean norm leads to a least square problem for which many specialized, efficient algorithms exist. Moreover, many statistical measures are based on the squared error, e.g., the coefficient of determination. The normalized error gives an equal weight to all deformation modes and does not overemphasize small stresses from very low and possibly noisy forces. The 1st Piola-Kirchhoff stress scales linearly w.r.t. the measured forces and does not need a conversion based on the strain measurement or assumption of perfect incompressibility. Thus, it allows a direct interpretation when testing or simulating the forces on the final rubber product. Furthermore, in contrast to the 2nd Piola-Kirchhoff stress, it is readily accessible for all deformation modes and does not lack of a physical meaning. Unlike the Cauchy stress, it does not give too much weight to the large strain regime which is of lower importance for most engineering applications.

4.2 Fitting of \bar{I}_1 -Dependent Strain Energy Functions

The fitting results of the strain energy functions depending only on \bar{I}_1 , cf. Tables 7 and 8, are given as bar charts in

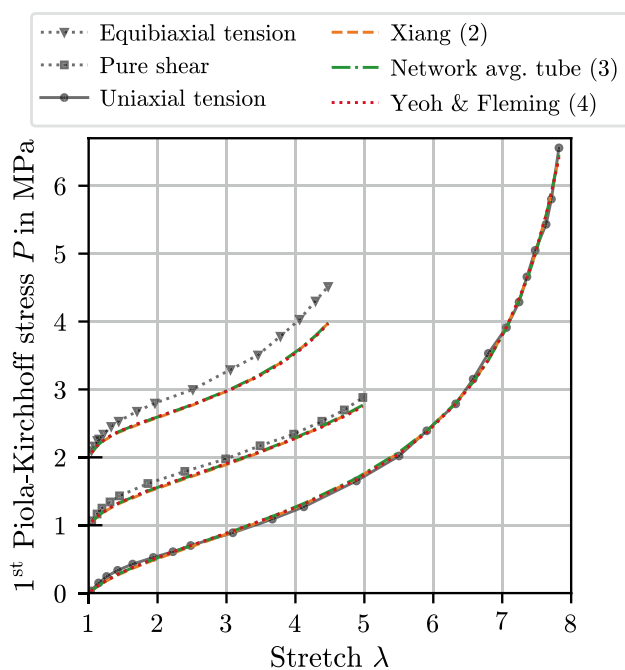


Fig. 19 Fitting of the best performing two-, three- and four-parameter \bar{I}_1 -model to the uniaxial tension data by Treloar [95] and their predictions for pure shear and equibiaxial tension (the stresses of the predictions are shifted by 1 and 2 MPa, respectively, for the sake of readability)

Figs. 10(a), 11(a), 12(a), 13(a), 14(a), 15(a), 16(a), 17(a) and 18(a). They show the root mean square error as well as the maximum error relative to the Neo-Hooke model for each compound. In addition, the stress-stretch plot of the best performing models with two, three, four and five parameters are given in Figs. 10(b), 11(b), 12(b), 13(b), 14(b), 15(b), 16(b), 17(b) and 18(b). These models are chosen for plotting rather than the overall top three models since the stress-stretch curves of the best ranked models nearly coincide for the most compounds and are hardly distinguishable.

Comparing the most promising candidates for each compound, it can be observed that there is not a best model which is generally applicable to all rubbers. However, counting the top three appearances, there are some strain energy functions with a high potential: the network averaging tube [58], Gregory [35], Beda [10], extended Yeoh [103] and Hoss and Marczak [47] model. The first one is a physically motivated model with only three parameters. It ranks first for two materials (BIIR+S, IR+S) and provides only for the CR+S compound unsatisfying results. In contrast, the others are phenomenological models with five parameters showing acceptable results for all compounds. However, for each material, there exist four- or three-parameter strain energy functions with a fitting quality nearly as good as the aforementioned ones. In general, models with a lower number of parameters are preferable to avoid overparametrization. That

is, they are prone to non-sensitive, non-unique and numerically undesirable parameters with a strong dependence on the initial guess, high correlations and a large number of iterations within in the fitting procedure.

Even models with two parameters are acceptable for some compounds. For example, they are suitable for materials that can stand comparatively low strains and exhibit no upturn, e.g., the peroxide-crosslinked rubbers. For the CR+P compound in Fig. 12, yet the Neo-Hooke model can be reasonable. Furthermore, the response of some sulfur-crosslinked compounds with large strains and a pronounced upturn can be captured acceptably with only two parameters, e.g., the BIIR+S, CR+S, NBR+S and SBR+S compound. Notably, in the authors' opinion, the stress-strain curves of these materials do not have any obvious property in common.

Looking into more detail for the sulfur-crosslinked compounds, two frequent shortcomings even of top-ranked models can be noticed. On the one hand, models typically fail to fit accurately the concave shape at small to moderate strains leading to an underestimation of the stress response in this region, see for instance Fig. 15(b). On the other hand, the material behavior close to the maximum strain is not reproduced properly by numerous models, e.g., the Swanson model in Fig. 14(b). Hence, the maximum error usually lies either in that small to moderate strain region or close to the failure strain. Since rubber parts are rarely designed for large deformations close to failure and the sample variance is high at very large strains, the former is considered as more critical. As discussed in Sect. 4.1.3, a residual with a 2nd Piola-Kirchhoff stress or a relative error can ease the shortcoming in the small strain regime to some extent.

The "a posteriori" check of monotonicity conditions, as discussed in Sect. 4.1.1, is passed by all strain energy functions except the extended Yeoh model. It violates monotonicity of the 1st Piola-Kirchhoff stress when calibrated for the IR+S compound. This issue is due to its exponential term, cf. Table 7, which is responsible for the good fit of the aforementioned concave shape. However, the exponential reduces faster than the polynomial terms increase such that the stress-stretch curve temporarily shows a slightly negative slope when changing from the concave to convex curvature.

4.3 Fitting of \bar{I}_2 -Dependent Strain Energy Functions

For the identification of promising \bar{I}_2 -dependent strain energy functions, the natural rubber from Treloar [95] is used since experimental data from multiple biaxial tensile tests are needed, cf. Sect. 4.1.2. First, all \bar{I}_1 -models from Tables 7 and 8 were fitted only to the uniaxial Treloar data to identify the best performing two-, three- and four-parameter \bar{I}_1 -model. These are the strain energy functions by Xiang et al. [100], Khiêm & Itskov [58] and Yeoh & Fleming [104] which show a very similar goodness of

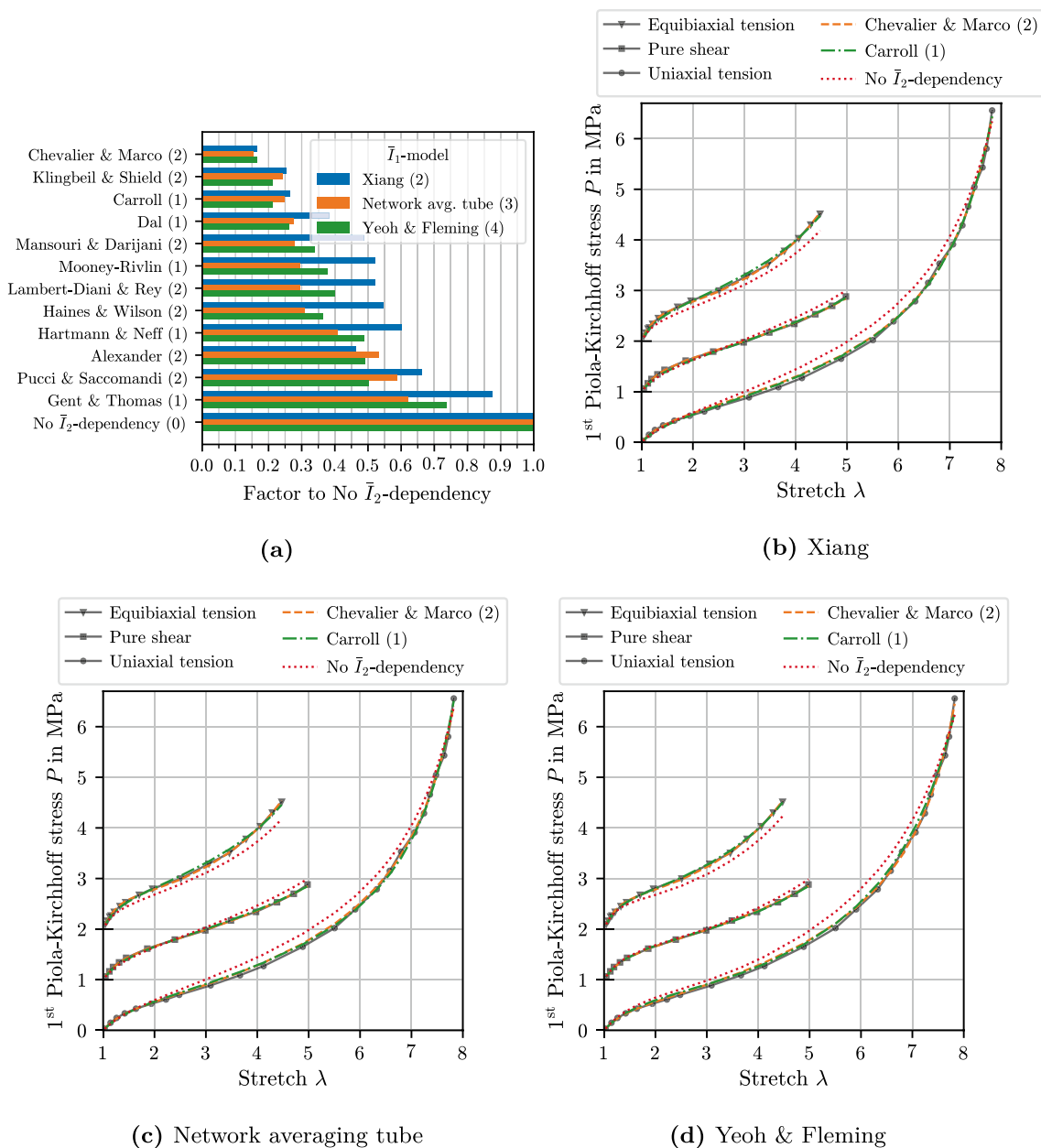


Fig. 20 a Ranking of the \bar{I}_2 -dependent strain energy functions for the Treloar data [95] (number of parameters is given in brackets); fitting of the best performing one- and two-parameter \bar{I}_2 -model as well as

the \bar{I}_2 -independent approach combined with the best ranked \bar{I}_1 -models with **b** two, **c** three and **d** four parameters

fit, cf. Fig. 19 for the resulting stress-strain curves. Each of the three \bar{I}_1 -models is then combined with all \bar{I}_2 -models from Table 9.

The results are depicted in Fig. 20. The additional \bar{I}_2 -dependency improves the fitting quality significantly for all three considered \bar{I}_1 -models. However, the degree of improvement depends on the combination of the \bar{I}_1 - and \bar{I}_2 -parts. For example, the \bar{I}_1 -model by Xiang et al. [100] almost always achieves the smallest improvement whereas the Network averaging tube model [58] benefits strongly from all

\bar{I}_2 -parts. Only when combined with the Alexander model, the Xiang model shows the largest improvement. Since such interdependencies between the \bar{I}_1 - and \bar{I}_2 -parts can hardly be foreseen, general conclusions for all \bar{I}_1 - \bar{I}_2 -combinations must be made carefully. More precisely, it is also possible that an \bar{I}_1 -model which performs poorly on its own may show great results with highly different parameter values when combined with a proper \bar{I}_2 -part.

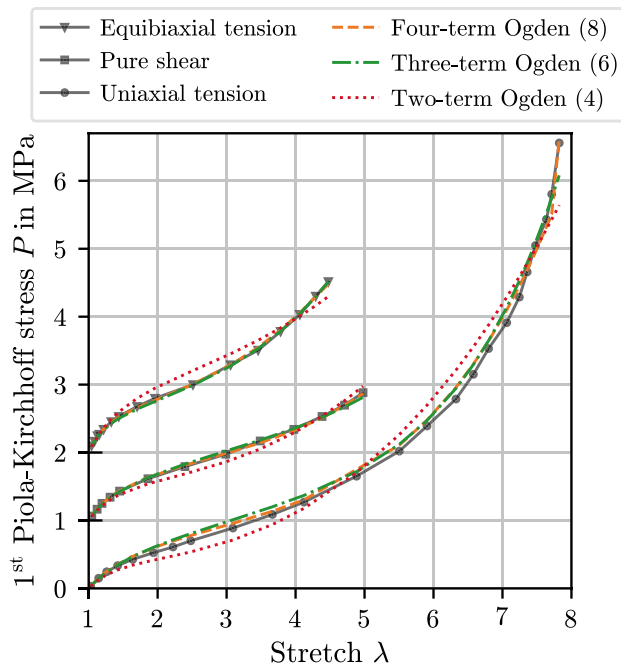


Fig. 21 Fitting of the Ogden model with two, three and four terms to the Treloar data [95] (number of parameters is given in brackets)

Another desirable feature of the \bar{I}_2 -models is the improved fit of the concave shape at low to moderate strains ($\lambda < 2$) of the uniaxial fits, cf. Fig. 19 and Sect. 4.2. This shortcoming is largely compensated when a \bar{I}_2 -part is added, cf. green and orange lines in Figs. 20(b-d). In case of the Yeoh & Fleming \bar{I}_1 -model, this effect can lead to anomalous parameters in the exponential term (i.e., negative B or large A , cf. Table 7) since this term is already designed to reproduce the behavior in this strain regime and, hence, loses its original purpose.

For all \bar{I}_1 -models, the \bar{I}_2 -part by Chevalier & Marco [18] provides the best improvement, followed by the Klingbeil & Shield approach [60]. Both strain energy functions require two additional parameters. For the latter, the exponent m determines whether $W_{\text{iso},2}$ is a concave ($m \leq 1$) or convex ($m \geq 1$) function. This parameter is fitted to $m = 0.46$ (Xiang), $m = 0.60$ (Network averaging tube) and $m = 0.48$ (Yeoh & Fleming), i.e., $W_{\text{iso},2}$ is always concave. The two best performing one-parameter \bar{I}_2 -models are special cases of this approach with $m = 1/2$ [16] and $m = 1/3$ [21] and, hence, concave functions, too. Furthermore, the aforementioned, top-ranked model by Chevalier & Marco [18] is concave as it is the sum of the two special cases $m = 1$ (Mooney-Rivlin, linear) and $m \rightarrow 0$ (Gent & Thomas, concave). Interestingly, these two cases on their own show only moderate results. Hartmann & Neff [38] introduced the exponent $m = 3/2$ to ensure polyconvexity for all deformation states but at the expense of fitting quality. In case of the Mansouri & Darijani model

[67], the parameter a was fitted to small negative values (order of magnitude -10^{-3}) implying slight concavity of $W_{\text{iso},2}$. Also, c_{02} of the Haines & Wilson model [36] was optimized to small negative values (-10^{-6}) resulting in a negligibly concave \bar{I}_2 -part. The exponent of the Lambert-Diani & Rey model [63] tends to the lower bound $m \rightarrow 1$, i.e., it reduces from a strictly convex function to the linear Mooney-Rivlin approach. Apparently, a concave \bar{I}_2 -dependency is essential for a good fit to several deformation modes. To prove this conclusion, the model $W_{\text{iso}} = c_{10}((\bar{I}_1/3)^{m_1} - 1) + c_{01}((\bar{I}_2/3)^{m_2} - 1)$, cf. [92], with a symmetric dependency on \bar{I}_1 and \bar{I}_2 was fitted to all three deformation modes of the Treloar data. The optimized parameters fulfill $c_{10} > 0$, $m_1 > 1$, $c_{01} > 0$, $0 < m_2 < 1$, i.e., a convex \bar{I}_1 - and a concave \bar{I}_2 -dependency.

The section closes with a comparison of the invariant-based models in Figs. 20(b-d) to the widely used, stretch-based Ogden model [78], viz.,

$$\omega(\bar{\lambda}_k) = \sum_{i=1}^n \frac{2\mu_i}{\alpha_i^2} (\bar{\lambda}_k^{\alpha_i} - 1) \quad , \quad (36)$$

cf. Eq. (23). Implementations with two, three and four terms ($n = 2, 3, 4$), i.e., four, six and eight parameters are considered. The fitting results in Fig. 21 reveal that at least three terms are needed for an accurate fit. Comparing the three- and four-term implementation, both exhibit similar stress responses for equibiaxial tension and pure shear. Only for the uniaxial load case at moderate strains ($2 < \lambda < 4$) and at very large strains ($\lambda > 7.5$), the model with four terms is superior. However, the four-term implementation with eight parameters shows signs of overparametrization, e.g., non-reproducible results from different initial guesses. In contrast, all model combinations in Figs. 20(b-d) with both \bar{I}_1 - and \bar{I}_2 -dependency can reproduce the experiments over the full strain range in all three deformation modes with less and unique material parameters. For instance, the Yeoh & Fleming model combined with the Chevalier & Marco \bar{I}_2 -term requires six parameters and the combination of the Xiang with the Carroll model leads to only three parameters in total.

5 Fitting of Volumetric Strain Energy Functions

The fitting of volumetric strain energy functions W_{vol} is more straightforward than the calibration of the isochoric models in the previous section. Due to the nearly linear material behavior, i.e., slightly convex pressure-volume curves, cf. Fig. 1(b), most of the models in the literature have one or two parameters. Moreover, W_{vol} is a function of only one argument J . That allows, in contrast to the isochoric strain

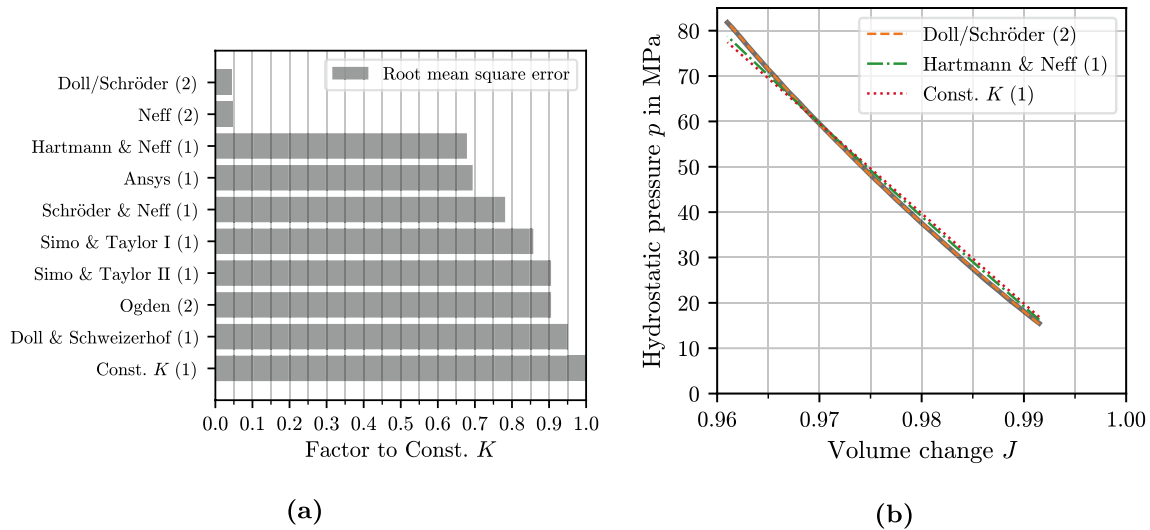


Fig. 22 Fitting results for the IR+S compound: **(a)** ranking sorted by RMSE, **(b)** pressure-volume curve of the best performing models with two and one parameters as well as the reference model with a

constant bulk modulus (experimental data are shown as grey, solid line; the number of parameters is given in brackets)

Table 10 Volumetric strain energy functions (n is the number of material parameters with restrictions on the second parameter β ; the initial bulk modulus K_0 must be positive for all models; comments on specific models: 6) both citations originally present three-parameter strain energy functions which are reduced here to the same two-parameter model, see also [83, 87])

No.	Name	Literature	Strain energy function W_{vol}	n
0	Const. K	–	$\frac{K_0}{2}(J - 1)^2$	1
1	Ogden	[79] Eq. (25)	$\frac{K_0}{\beta^2}(-\beta \ln(J) + J^\beta - 1)$	$2 (\beta \geq 2)$
2	Simo & Taylor I	[89] Eq. (29)	$\frac{K_0}{4}(\ln(J)^2 + (J - 1)^2)$	1
3	Simo & Taylor II	[90] Eq. (4.34) ₂	$\frac{K_0}{4}(-2 \ln(J) + J^2 - 1)$	1
4	Ansys	[2] Eq. (4.5–4)	$\frac{K_0}{32}(J^4 + \frac{1}{J^4} - 2)$	1
5	Doll & Schweizerhof	[26] Eq. (16) ₁	$\frac{K_0}{2}(\exp(J - 1) - \ln(J) - 1)$	1
6	Doll/Schröder	[26] Eq. (13)/ [86] Eq. (3.33) ₂	$\frac{K_0}{2\beta^2}(J^\beta + \frac{1}{J^\beta} - 2)$	$2 (\beta \geq 2)$
7	Schröder & Neff	[86] Eq. (3.33) ₅	$\frac{K_0}{12}(4 \ln(J)^2 - 2 \ln(J) + J^2 - 1)$	1
8	Hartmann & Neff	[38] Eq. (3.2)	$\frac{K_0}{50}(J^5 + \frac{1}{J^5} - 2)$	1
9	Neff	[77] Eq. (1.4) ₂	$\frac{K_0}{2\beta}(\exp(\beta \ln(J)^2) - 1)$	$2 (\beta \geq 1)$

energy functions, a simple ”a priori“ imposition of reasonable parameter limits. In total, 23 models were found in the literature, cf. [84], but only nine of them, cf. Table 10, fulfill the following requirements:

- Strict convexity, i.e., a positive bulk modulus (even for $J \rightarrow \infty$): $K = \partial^2 W_{vol} / \partial J^2 > 0$
- Non-finite response when approaching zero volume: $J \rightarrow 0 \Rightarrow W_{vol} \rightarrow \infty$
- Stress-free state at undeformed configuration: $J = 1 \Rightarrow \partial W_{vol} / \partial J = 0$ (implies that if W_{vol} is strict convex, then $J = 1$ is its global minimum)
- Maximum two parameters

Although it violates the second requirement, the widely used strain energy with a constant bulk modulus is taken as reference. For the two-parameter models, a lower bound for the second parameter β , cf. Table 10, is prescribed to ensure that the aforementioned restrictions are always fulfilled. It is worth mentioning that the first three requirements are numerically motivated rather than physically. More specific, the validity of the considered models is bounded on the one hand by cavitation damage which can be observed for $J > 1$, see for instance [27]. On the other hand, hydrostatic compression ($J < 1$) can lead to pressure-induced glass transition [17]. Both phenomena cause a significant change of the material properties and cannot be captured by the models. Hence, a discussion for $J \rightarrow \infty$ or $J \rightarrow 0$ is actually meaningless from a physical point of view. Moreover, if cavitation

damage is to be modeled, the strict convexity requirement can be violated and has to be abandoned.

The results are very similar for all compounds. Therefore, they are exemplified by means of the IR+S compound in Fig. 22 and those for the remaining materials are given in App. E. For all materials, the two-parameter models by Doll & Schweizerhof [26]/Schröder & Neff [86] and Neff et al. [77] show the best results. However, for both models, the second parameter β takes large values ($\beta > 18$ for Doll/Schröder and $\beta > 57$ for Neff, cf. Table 10). Since this parameter appears in the exponent and adjusts the curvature of the pressure-volume curve, it can readily affect the stability of finite element simulations. Hence, specialized elements are required, see for instance [87]. The third two-parameter model by Ogden [79] reduces for all materials to the Simo & Taylor II model with the limiting case $\beta \rightarrow 2$. Here, greater β -values would generate a less convex or even concave curvature of the pressure-volume curve.

The one-parameter models fail to reproduce the curvature of the experimental data and show moderate fitting quality. For instance, the top-ranked Ansys model [2] and Hartmann & Neff model [38] are special cases of the Doll/Schröder model by fixing the second parameter. However, the fixed β -values are too small to properly reproduce the experimental data (fixed $\beta = 4$ and $\beta = 5$ vs. fitted $\beta = 18 \dots 42$). In general, the gain in fitting quality of the one-parameter models in comparison to the reference approach with a constant bulk modulus is comparatively small. Hence, in practice, the possibly little improvement of the fit must be weighted up against the numerical robustness of a constant bulk modulus. Moreover, the confined compression test is always subjected to friction, cf. [83, 50], such that the modulus and the curvature of the experimental pressure-volume curve tend to be overestimated.

6 Conclusion

The present manuscript provides a guideline for the process of model selection and calibration of hyperelastic models for rubber materials. For this purpose, the paper begins with a discussion on crucial aspects of the preparation of the experimental data. That includes the proposition of physically motivated procedures for the preload correction in tensile and compression tests. Moreover, a consistency check for multiple experiments in different deformation modes is derived. It was shown that the presented preload correction is a suitable approach to compensate an improper preload. The consistency check was applied to the widely used Treloar data [95] proving a good agreement between its uniaxial tensile, pure shear and equibiaxial tensile test.

Then, the importance of the \bar{I}_2 -contribution to the strain energy function for an accurate and plausible model behavior

in several deformation modes is pointed out and illustrated. However, models depending on both \bar{I}_1 and \bar{I}_2 show a limited predictivity to other deformation modes when fitted to only one experiment. Furthermore, the effect of different cost function formulations (i.e., stress measure, error type and order of the residual norm) on the fitting result is demonstrated. This choice can strongly affect the fitting results and cause different rankings. It allows to design tailor-made cost functions which emphasize particular strain regimes or deformation modes.

Based on this preliminary work, 33 strain energy functions in terms of \bar{I}_1 were fitted to uniaxial tension data of nine different rubber compounds. The models with the largest number of material parameters are able to reproduce the stress response of most of the materials, e.g., the extended Yeoh [103], Beda [10], Gregory [35] or Hoss & Marczak [47] model with five parameters each. However, they often tend to numerically undesirable parameters and a slow optimization procedure. In contrast, strain energy functions with three or four parameters, like the network average tube model [58], show satisfying results for specific compounds but are less generally applicable. Two-parameter models provide acceptable fittings for the two peroxide cross-linked rubbers, which exhibit the smallest elongation at break, and for a few of the sulfur cross-linked compounds.

For the identification of promising \bar{I}_2 -based strain energy functions, the Treloar data were considered. The best-performing one-, two and three-parameter \bar{I}_1 -model were combined with twelve \bar{I}_2 -approaches. It was observed that concave \bar{I}_2 -dependent strain energy functions with a moderate curvature are well suited to improve the goodness of fit, e.g., the Chevalier & Marco [18] or Carroll model [16] with two and one parameter, respectively. More precisely, the additional \bar{I}_2 -dependency is able to balance the stress response of different deformation modes and can compensate shortcomings of a pure \bar{I}_1 -dependency. However, since the test framework considers those \bar{I}_1 -models which perform already well on their own, these findings do not allow general statements about preferable \bar{I}_2 -approaches.

Finally, modeling approaches for the volumetric behavior were analyzed. For this purpose, nine strain energy functions are fitted to the confined compression data of the nine above-mentioned rubber compounds. In contrast to the stress-strain curves of the uniaxial tensile test, the pressure-volume curves of all materials are very similar. Hence, suitable volumetric strain energy functions are ranked similarly, too. Clearly, the two-parameter models Doll/Schröder [26, 86] and Neff [77] provide the best results. However, their pronounced non-linearity may lead to additional numerical challenges.

For future work, an expansion of the presented database is reasonable. More precisely, up-to-date data sets comprised of uniaxial tensile, pure shear and equibiaxial tensile tests on several compounds are desirable. This would

allow well-founded investigations of further \bar{I}_1 - \bar{I}_2 model combinations, of coupled \bar{I}_1 - \bar{I}_2 -terms and of stretch-based models. Alternatively, general biaxial tension data could be employed for these purposes. In that case, discussions on the preparation and on the consistency check of the data as well as on the treatment of two stress values in the cost function are necessary. Furthermore, the accuracy and error sources of the biaxial experimental setup should be assessed.

Supplementary Information The online version contains supplementary material available at <https://doi.org/10.1007/s11831-022-09865-x>.

Acknowledgements The authors would like to thank Jan Plagge, Deutsches Institut für Kautschuktechnologie e.V., Hannover for the fruitful discussion on the data preparation section. Moreover, the constructive and helpful feedback on the manuscript by Meike Gierig, Leibniz University Hannover, is highly appreciated.

Funding Open Access funding enabled and organized by Projekt DEAL.

Declarations

Conflict of interest On behalf of all authors, the corresponding author states that there is no conflict of interest.

Open Access This article is licensed under a Creative Commons Attribution 4.0 International License, which permits use, sharing, adaptation, distribution and reproduction in any medium or format, as long as you give appropriate credit to the original author(s) and the source, provide a link to the Creative Commons licence, and indicate if changes were made. The images or other third party material in this article are included in the article's Creative Commons licence, unless indicated otherwise in a credit line to the material. If material is not included in the article's Creative Commons licence and your intended use is not permitted by statutory regulation or exceeds the permitted use, you will need to obtain permission directly from the copyright holder. To view a copy of this licence, visit <http://creativecommons.org/licenses/by/4.0/>.

References

- Alexander H (1968) A constitutive relation for rubber-like materials. *Int J Eng Sci* 6(9):549–563. [https://doi.org/10.1016/0020-7225\(68\)90006-2](https://doi.org/10.1016/0020-7225(68)90006-2)
- ANSYS, Inc. (1999) ANSYS theory reference release 5.6
- Arruda EM, Boyce MC (1993) A three-dimensional constitutive model for the large stretch behavior of rubber elastic materials. *J Mech Phys Solids* 41(2):389–412. [https://doi.org/10.1016/0022-5096\(93\)90013-6](https://doi.org/10.1016/0022-5096(93)90013-6)
- Baaser H, Hopmann C, Schobel A (2013) Reformulation of strain invariants at incompressibility. *Arch Appl Mech* 83(2):273–280. <https://doi.org/10.1007/s00419-012-0652-2>
- Baker M, Ericksen JL (1954) Inequalities restricting the form of the stress-deformation relations for isotropic elastic solids and reiner-rivlin fluids. *J Wash Acad Sci* 44(2):33–35
- Ball JM (1976) Convexity conditions and existence theorems in nonlinear elasticity. *Arch Ration Mech Anal* 63(4):337–403. <https://doi.org/10.1007/bf00279992>
- Beatty MF (1987) Topics in finite elasticity: hyperelasticity of rubber, elastomers, and biological tissues—with examples. *Appl Mech Rev* 40(12):1699–1734. <https://doi.org/10.1115/1.3149545>
- Beatty MF (2007) On constitutive models for limited elastic, molecular based materials. *Math Mech Solids* 13(5):375–387. <https://doi.org/10.1177/1081286507076405>
- Becker GW (1967) On the phenomenological description of the nonlinear deformation behavior of rubberlike high polymers. *J Polym Sci Polym Symp* 16(5):2893–2903. <https://doi.org/10.1002/polc.5070160543>
- Beda T (2004) Reconciling the fundamental phenomenological expression of the strain energy of rubber with established experimental facts. *J Polym Sci B: Polym Phys* 43(2):125–134. <https://doi.org/10.1002/polb.20308>
- Beda T (2014) An approach for hyperelastic model-building and parameters estimation a review of constitutive models. *Eur Polym J* 50:97–108. <https://doi.org/10.1016/j.eurpolymj.2013.10.006>
- bin Othman A, Gregory MJ (1990) A stress-strain relationship for filled rubber. *J Nat Rubber Res* 5(2):144–155
- Boyce MC, Arruda EM (2000) Constitutive models of rubber elasticity: a review. *Rubber Chem Technol* 73(3):504–523. <https://doi.org/10.5254/1.3547602>
- Bronshstein IN, Semendyayev KA, Musiol G, Muehlig H (2007) *Handbook of mathematics*, 5th edn. Springer, Berlin, Heidelberg
- Budday S, Sommer G, Haybaeck J, Steinmann P, Holzapfel GA, Kuhl E (2017) Rheological characterization of human brain tissue. *Acta Biomater* 60:315–329. <https://doi.org/10.1016/j.actbio.2017.06.024>
- Carroll MM (2010) A strain energy function for vulcanized rubbers. *J Elast* 103(2):173–187. <https://doi.org/10.1007/s10659-010-9279-0>
- Champagne J, Cantournet S, Colombo D, Jamonneau S, Le Gorju K, Lequeux F, Montes H (2020) Role of glassy bridges on the mechanics of filled rubbers under pressure. *Macromolecules* 53(10):3728–3737. <https://doi.org/10.1021/acs.macromol.0c00395>
- Chevalier L, Marco Y (2002) Tools for multiaxial validation of behavior laws chosen for modeling hyper-elasticity of rubberlike materials. *Polym Eng Sci* 42(2):280–298. <https://doi.org/10.1002/pen.10948>
- Cohen A (1991) A Padé approximant to the inverse langevin function. *Rheol Acta* 30(3):270–273. <https://doi.org/10.1007/bf00366640>
- Dal H, Badienia Y, Açıkgöz K, Aksu Denli F (2019) A comparative study on hyperelastic constitutive models on rubber: state of the art after 2006. In: Huneau B, Le Cam JB, Marco Y, Verron E (eds) *Proceedings of the ECCMR XI*. CRC Press, pp 239–244
- Dal H, Gültekin O, Açıkgöz K (2020) An extended eight-chain model for hyperelastic and finite viscoelastic response of rubberlike materials: theory, experiments and numerical aspects. *J Mech Phys Solids* 145:104159. <https://doi.org/10.1016/j.jmps.2020.104159>
- Dal H, Açıkgöz K, Badienia Y (2021) On the performance of isotropic hyperelastic constitutive models for rubber-like materials: a state of the art review. *Appl Mech Rev*. <https://doi.org/10.1115/1.4050978>
- Davies CKL, De DK, Thomas AG (1994) Characterization of the behavior of rubber for engineering design purposes. 1. Stress-strain relations. *Rubber Chem Technol* 67(4):716–728. <https://doi.org/10.5254/1.3538706>
- Destrade M, Saccomandi G, Sgura I (2017) Methodical fitting for mathematical models of rubber-like materials. *Proc R Soc*

- A 473(2198):20160811. <https://doi.org/10.1098/rspa.2016.0811>
25. Dobrynin AV, Carrillo J-MY (2011) Universality in nonlinear elasticity of biological and polymeric networks and gels. *Macromolecules* 44(1):140–146. <https://doi.org/10.1021/ma102154u>
 26. Doll S, Schweizerhof K (2000) On the development of volumetric strain energy functions. *J Appl Mech* 67(1):17–21. <https://doi.org/10.1115/1.321146>
 27. Dorfmann A, Fuller KNG, Ogden RW (2002) Shear, compressive and dilatational response of rubberlike solids subject to cavitation damage. *Int J Solids Struct* 39(7):1845–1861. [https://doi.org/10.1016/s0020-7683\(02\)00008-2](https://doi.org/10.1016/s0020-7683(02)00008-2)
 28. Drucker DC (1959) A definition of stable inelastic material. *J Appl Mech* 26(1):101–106. <https://doi.org/10.1115/1.4011929>
 29. Edwards SF, Vilgis T (1986) The effect of entanglements in rubber elasticity. *Polymer* 27(4):483–492. [https://doi.org/10.1016/0032-3861\(86\)90231-4](https://doi.org/10.1016/0032-3861(86)90231-4)
 30. Fu X, Wang Z, Ma L (2021) Ability of constitutive models to characterize the temperature dependence of rubber hyperelasticity and to predict the stress-strain behavior of filled rubber under different deformation states. *Polymers* 13(3):369. <https://doi.org/10.3390/polym13030369>
 31. Gent AN (1996) A new constitutive relation for rubber. *Rubber Chem Technol* 69(1):59–61. <https://doi.org/10.5254/1.3538357>
 32. Gent AN, Thomas AG (1958) Forms for the stored (strain) energy function for vulcanized rubber. *J Polym Sci* 28(118):625–628. <https://doi.org/10.1002/pol.1958.1202811814>
 33. Gorash Y, Comlekci T, Hamilton R (2015) CAE-based application for identification and verification of hyperelastic parameters. *Proc Inst Mech Eng L* 231(7):611–626. <https://doi.org/10.1177/1464420715604004>
 34. Gottlieb M, Gaylord RJ (1987) Experimental tests of entanglement models of rubber elasticity. 3. Biaxial deformations. *Macromolecules* 20(1):130–138. <https://doi.org/10.1021/ma00167a022>
 35. Gregory IH, Muhr AH, Stephens IJ (1997) Engineering applications of rubber in simple extension. *Plast Rubber Compos Process Appl* 26(3):117–122
 36. Haines DW, Wilson WD (1979) Strain-energy density function for rubberlike materials. *J Mech Phys Solids* 27(4):345–360. [https://doi.org/10.1016/0022-5096\(79\)90034-6](https://doi.org/10.1016/0022-5096(79)90034-6)
 37. Hart-Smith LJ (1966) Elasticity parameters for finite deformations of rubber-like materials. *ZAMP* 17(5):608–626. <https://doi.org/10.1007/bf01597242>
 38. Hartmann S, Neff P (2003) Polyconvexity of generalized polynomial-type hyperelastic strain energy functions for near-incompressibility. *Int J Solids Struct* 40(11):2767–2791. [https://doi.org/10.1016/s0020-7683\(03\)00086-6](https://doi.org/10.1016/s0020-7683(03)00086-6)
 39. Haupt P (2002) *Continuum mechanics and theory of materials*. Springer, Berlin, Heidelberg. <https://doi.org/10.1007/978-3-662-04775-0>
 40. Haupt P, Sedlan K (2001) Viscoplasticity of elastomeric materials: experimental facts and constitutive modelling. *Arch Appl Mech* 71(2–3):89–109. <https://doi.org/10.1007/s004190000102>
 41. He H, Zhang Q, Zhang Y, Chen J, Zhang L, Li F (2021) A comparative study of 85 hyperelastic constitutive models for both unfilled rubber and highly filled rubber nanocomposite material. *Nano Mater Sci*. <https://doi.org/10.1016/j.nanoms.2021.07.003>
 42. Heinrich G, Kaliske M (1997) Theoretical and numerical formulation of a molecular based constitutive tube-model of rubber elasticity. *Comput Theor Polym Sci* 7(3–4):227–241. [https://doi.org/10.1016/s1089-3156\(98\)00010-5](https://doi.org/10.1016/s1089-3156(98)00010-5)
 43. Heuillet P, Dugautier L (1997) Modélisation du comportement hyperélastique des caoutchoucs et élastomères thermoplastiques, compacts ou cellulaires. In: *Génie mécanique des caoutchoucs et des élastomères thermoplastiques*, pp 67–103
 44. Hill R (1958) A general theory of uniqueness and stability in elastic-plastic solids. *J Mech Phys Solids* 6(3):236–249. [https://doi.org/10.1016/0022-5096\(58\)90029-2](https://doi.org/10.1016/0022-5096(58)90029-2)
 45. Hohenberger TW, Windslow RJ, Pugno NM, Busfield JJC (2019) A constitutive model for both low and high strain nonlinearities in highly filled elastomers and implementation with user-defined material subroutines in Abaqus. *Rubber Chem Technol* 92(4):653–686. <https://doi.org/10.5254/rct.19.80387>
 46. Horgan CO, Saccomandi G (2006) Phenomenological hyperelastic strain-stiffening constitutive models for rubber. *Rubber Chem Technol* 79(1):152–169. <https://doi.org/10.5254/1.3547924>
 47. Hoss L, Marczak RJ (2009) A new constitutive model for rubber-like materials. In: *Proceedings of the 20th COBEM*
 48. Hossain M, Steinmann P (2013) More hyperelastic models for rubber-like materials: consistent tangent operators and comparative study. *J Mech Behav Mater* 22(1–2):27–50. <https://doi.org/10.1515/jmbm-2012-0007>
 49. Hossain M, Amin AFMS, Kabir MN (2015) Eight-chain and full-network models and their modified versions for rubber hyperelasticity: a comparative study. *J Mech Behav Mater* 24(1–2):11–24. <https://doi.org/10.1515/jmbm-2015-0002>
 50. IIseng A, Skallerud BH, Clausen AH (2015) Volumetric compression of HNBR and FKM elastomers. In: Marvalová B, Petriková I (eds) *Proceedings of the ECCMR IX*. CRC Press, pp 235–241
 51. Isihara A, Hashitume N, Tatibana M (1951) Statistical theory of rubber-like elasticity IV. Two-dimensional stretching. *J Chem Phys* 19(12):1508–1512. <https://doi.org/10.1063/1.1748111>
 52. James AG, Green A, Simpson GM (1975) Strain energy functions of rubber I. Characterization of gum vulcanizates. *J Appl Polym Sci* 19(7):2033–2058. <https://doi.org/10.1002/app.1975.070190723>
 53. Jones DF, Treloar LRG (1975) The properties of rubber in pure homogeneous strain. *J Phys D Appl Phys* 8(11):1285–1304. <https://doi.org/10.1088/0022-3727/8/11/007>
 54. Kaliske M, Heinrich G (1999) An extended tube-model for rubber elasticity: statistical-mechanical theory and finite element implementation. *Rubber Chem Technol* 72(4):602–632. <https://doi.org/10.5254/1.3538822>
 55. Kawabata S, Kawai H (1977) Strain energy density functions of rubber vulcanizates from biaxial extension. In: *Molecular properties*. Springer, Berlin, Heidelberg, pp 89–124. https://doi.org/10.1007/3-540-08124-0_2
 56. Kawabata S, Matsuda M, Tei K, Kawai H (1981) Experimental survey of the strain energy density function of isoprene rubber vulcanizate. *Macromolecules* 14(1):154–162. <https://doi.org/10.1021/ma50002a032>
 57. Khajehsaeid H, Arghavani J, Naghdabadi R (2013) A hyperelastic constitutive model for rubber-like materials. *Eur J Mech A Solids* 38:144–151. <https://doi.org/10.1016/j.euromechsol.2012.09.010>
 58. Khiêm VN, Itskov M (2016) Analytical network-averaging of the tube model: rubber elasticity. *J Mech Phys Solids* 95:254–269. <https://doi.org/10.1016/j.jmps.2016.05.030>
 59. Kilian H-G (1985) An interpretation of the strain-invariants in largely strained networks. *Colloid Polym Sci* 263(1):30–34. <https://doi.org/10.1007/bf01411245>
 60. Klingbeil WW, Shield RT (1964) Some numerical investigations on empirical strain energy functions in the large axis-symmetric extensions of rubber membranes. *ZAMP* 15(6):608–629. <https://doi.org/10.1007/bf01595147>
 61. Knowles JK (1977) The finite anti-plane shear field near the tip of a crack for a class of incompressible elastic solids. *Int J Fract* 13(5):611–639. <https://doi.org/10.1007/bf00017296>
 62. Korelc J, Wriggers P (2016) *Automation of finite-element-methods*. Springer, Switzerland

63. Lambert-Diani J, Rey C (1999) New phenomenological behavior laws for rubbers and thermoplastic elastomers. *Eur J Mech A Solids* 18(6):1027–1043. [https://doi.org/10.1016/s0997-7538\(99\)00147-3](https://doi.org/10.1016/s0997-7538(99)00147-3)
64. Lim GT (2005) Scratch behavior of polymers. PhD thesis, Texas A&M University
65. Lion A (1997) A physically based method to represent the thermo-mechanical behaviour of elastomers. *Acta Mech* 123(1–4):1–25. <https://doi.org/10.1007/bf01178397>
66. Liu CH, Mang HA (1996) A critical assessment of volumetric strain energy functions for hyperelasticity at large strains. *ZAMM* 76(S5):301–350. <https://doi.org/10.1002/zamm.19960761509>
67. Mansouri MR, Darijani H (2014) Constitutive modeling of isotropic hyperelastic materials in an exponential framework using a self-contained approach. *Int J Solids Struct* 51(25–26):4316–4326. <https://doi.org/10.1016/j.ijsolstr.2014.08.018>
68. Marckmann G, Verron E (2006) Comparison of hyperelastic models for rubber-like materials. *Rubber Chem Technol* 79(5):835–858. <https://doi.org/10.5254/1.3547969>
69. Marsden JE, Hughes TJR (1994) *Mathematical foundations of elasticity*. Dover Publications, New York
70. Martins PALS, Jorge RMN, Ferreira AJM (2006) A comparative study of several material models for prediction of hyperelastic properties: application to silicone-rubber and soft tissues. *Strain* 42(3):135–147. <https://doi.org/10.1111/j.1475-1305.2006.00257.x>
71. Meier P, Khader S, Preuß R, Dietrich J, Voges D (2003) Uniaxial and equi-biaxial tension tests of silicone elastomer. In: Busfield J, Muhr A (eds) *Proceedings of the ECCMR III*. A.A. Balkema Publishers, pp 99–106
72. Meunier L, Chagnon G, Favier D, Orgéas L, Vacher P (2008) Mechanical experimental characterisation and numerical modelling of an unfilled silicone rubber. *Polym Test* 27(6):765–777. <https://doi.org/10.1016/j.polymertesting.2008.05.011>
73. Miehe C, Göktepe S, Lulei F (2004) A micro-macro approach to rubber-like materials—part I: the non-affine micro-sphere model of rubber elasticity. *J Mech Phys Solids* 52(11):2617–2660. <https://doi.org/10.1016/j.jmps.2004.03.011>
74. Mihai LA, Goriely A (2017) How to characterize a nonlinear elastic material? A review on nonlinear constitutive parameters in isotropic finite elasticity. *Proc R Soc A* 473(2207):20170607. <https://doi.org/10.1098/rspa.2017.0607>
75. Mihai LA, Chin L, Janmey PA, Goriely A (2015) A comparison of hyperelastic constitutive models applicable to brain and fat tissues. *J R Soc Interface* 12(110):20150486. <https://doi.org/10.1098/rsif.2015.0486>
76. Mooney M (1940) A theory of large elastic deformation. *J Appl Phys* 11(9):582–592. <https://doi.org/10.1063/1.1712836>
77. Neff P, Ghiba I-D, Lankeit J (2015) The exponentiated Hencky-logarithmic strain energy. Part I: constitutive issues and rank-one convexity. *J Elast* 121(2):143–234. <https://doi.org/10.1007/s10659-015-9524-7>
78. Ogden RW (1972) Large deformation isotropic elasticity—on the correlation of theory and experiment for incompressible rubber-like solids. *Proc R Soc A* 326(1567):565–584. <https://doi.org/10.1098/rspa.1972.0026>
79. Ogden RW (1972) Large deformation isotropic elasticity: on the correlation of theory and experiment for compressible rubber-like solids. *Proc R Soc A* 328(1575):567–583. <https://doi.org/10.1098/rspa.1972.0096>
80. Ogden RW (1997) *Non-linear elastic deformations*. Dover Publications, New York
81. Plagge J, Ricker A, Kröger NH, Wriggers P, Klüppel M (2020) Efficient modeling of filled rubber assuming stress-induced microscopic restructurization. *Int J Eng Sci* 151:103291. <https://doi.org/10.1016/j.ijengsci.2020.103291>
82. Pucci E, Saccomandi G (2002) A note on the gent model for rubber-like materials. *Rubber Chem Technol* 75(5):839–852. <https://doi.org/10.5254/1.3547687>
83. Ricker A, Kröger NH (2019) Influence of various curing systems and carbon black content on the bulk modulus of EPDM rubber. In: Huneau B, Le Cam JB, Marco Y, Verron E (eds) *Proceedings of the ECCMR XI*. CRC Press, pp 200–205
84. Ricker A, Fehse A, Kröger NH (2020) Charakterisierung sowie Modellbildung zur Beschreibung von Kompressionsmoduln technischer Gummiwerkstoffe. Schlussbericht zu IGF-Vorhaben Nr. 19916 N, Deutsches Institut für Kautschuktechnologie e.V.
85. Rivlin RS, Saunders DW (1951) Large elastic deformations of isotropic materials. VII. Experiments on the deformation of rubber. *Philos Trans R Soc A* 243(865):251–288. <https://doi.org/10.1098/rsta.1951.0004>
86. Schröder J, Neff P (2003) Invariant formulation of hyperelastic transverse isotropy based on polyconvex free energy functions. *Int J Solids Struct* 40(2):401–445. [https://doi.org/10.1016/s0020-7683\(02\)00458-4](https://doi.org/10.1016/s0020-7683(02)00458-4)
87. Schönherr JA, Schneider P, Mittelstedt C (2022) Robust hybrid/mixed finite elements for rubber-like materials under severe compression. *Comput Mech*. <https://doi.org/10.1007/s00466-022-02157-y>
88. Seibert DJ, Schöche N (2000) Direct comparison of some recent rubber elasticity models. *Rubber Chem Technol* 73(2):366–384. <https://doi.org/10.5254/1.3547597>
89. Simo JC, Taylor RL (1982) Penalty function formulations for incompressible nonlinear elastostatics. *Comput Methods Appl Mech Eng* 35(1):107–118. [https://doi.org/10.1016/0045-7825\(82\)90035-4](https://doi.org/10.1016/0045-7825(82)90035-4)
90. Simo JC, Taylor RL (1991) Quasi-incompressible finite elasticity in principal stretches. Continuum basis and numerical algorithms. *Comput Methods Appl Mech Eng* 85(3):273–310. [https://doi.org/10.1016/0045-7825\(91\)90100-k](https://doi.org/10.1016/0045-7825(91)90100-k)
91. Steinmann P, Hossain M, Possart G (2012) Hyperelastic models for rubber-like materials: consistent tangent operators and suitability for Treloar’s data. *Arch Appl Mech* 82(9):1183–1217. <https://doi.org/10.1007/s00419-012-0610-z>
92. Swanson SR (1985) A constitutive model for high elongation elastic materials. *J Eng Mater Technol* 107(2):110–114. <https://doi.org/10.1115/1.3225782>
93. Thiel C, Voss J, Martin RJ, Neff P (2019) Shear, pure and simple. *Int J Non Linear Mech* 112:57–72. <https://doi.org/10.1016/j.ijnonlinmec.2018.10.002>
94. Timbrell C, Wiehahn M, Cook G, Muhr AH (2003) Simulation of crack propagation in rubber. In: Busfield J, Muhr A (eds) *Proceedings of the ECCMR III*. A.A. Balkema Publishers, pp 11–20
95. Treloar LRG (1944) Stress-strain data for vulcanised rubber under various types of deformation. *Trans Faraday Soc* 40:59. <https://doi.org/10.1039/tf9444000059>
96. Vahapoğlu V, Karadeniz S (2006) Constitutive equations for isotropic rubber-like materials using phenomenological approach: a bibliography (1930–2003). *Rubber Chem Technol* 79(3):489–499. <https://doi.org/10.5254/1.3547947>
97. Valanis KC, Landel RF (1967) The strain-energy function of a hyperelastic material in terms of the extension ratios. *J Appl Phys* 38(7):2997–3002. <https://doi.org/10.1063/1.1710039>
98. Vangerko H, Treloar LRG (1978) The inflation and extension of rubber tube for biaxial strain studies. *J Phys D Appl Phys* 11(14):1969–1978. <https://doi.org/10.1088/0022-3727/11/14/009>
99. Wall FT (1942) Statistical thermodynamics of rubber II. *J Chem Phys* 10(7):485–488. <https://doi.org/10.1063/1.1723753>

100. Xiang Y, Zhong D, Wang P, Mao G, Yu H, Qu S (2018) A general constitutive model of soft elastomers. *J Mech Phys Solids* 117:110–122. <https://doi.org/10.1016/j.jmps.2018.04.016>
101. Yamashita Y, Kawabata S (1992) Approximated form of the strain energy-density function of carbon-black filled rubbers for industrial applications. *Nippon Gomu Kyokaishi* 65(9):517–528. <https://doi.org/10.2324/gomu.65.517>
102. Yeoh OH (1990) Characterization of elastic properties of carbon-black-filled rubber vulcanizates. *Rubber Chem Technol* 63(5):792–805. <https://doi.org/10.5254/1.3538289>
103. Yeoh OH (1993) Some forms of the strain energy function for rubber. *Rubber Chem Technol* 66(5):754–771. <https://doi.org/10.5254/1.3538343>
104. Yeoh OH, Fleming PD (1997) A new attempt to reconcile the statistical and phenomenological theories of rubber elasticity. *J Polym Sci B: Polym Phys* 35(12):1919–1931. [https://doi.org/10.1002/\(SICI\)1099-0488\(19970915\)35:12<1919::AID-POLB7>3.0.CO;2-K](https://doi.org/10.1002/(SICI)1099-0488(19970915)35:12<1919::AID-POLB7>3.0.CO;2-K)
105. Zhao Z, Mu X, Du F (2019) Modeling and verification of a new hyperelastic model for rubber-like materials. *Math Probl Eng* 1–10:2019. <https://doi.org/10.1155/2019/2832059>

Publisher's Note Springer Nature remains neutral with regard to jurisdictional claims in published maps and institutional affiliations.